ACCRETION DISK IN THE MASSIVE CLOSE BINARY STARS

GOJKO ĐJURAŠEVIĆ

STELLAR PHYSICS GROUP (ON176004)
ASTRONOMICAL OBSERVATORY BELGRADE

E-MAIL:

GDJURASEVIC@AOB.RS

About us

People in the group

- *G. Đurašević (founder), A. Cséki (administrator), S. Jankov, O. Atanacković, I. Vince, V. Čadež, B. Arbutina, O. Vince, I. Milić, M. Jurković, O. Latković, J. Petrović, S. Lazarević*

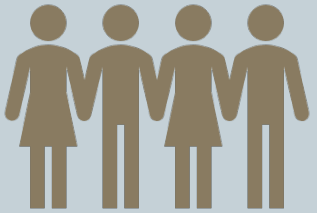

Areas of interest

- *Close binary stars modeling and evolution*
- *Numerical methods in radiation transfer; transfer of polarized radiation*
- *Stellar oscillations in single and binary stars; stellar rotation and the Be phenomenon*

About this talk

- Binary stars as the main origin of the fundamental stellar parameters in astrophysics
- We use our own modeling tools
- Recent topics

  Modeling of the massive CBS
  - *Double-periodic variables*
  - Evolution status of these systems
- Future research
  - *Innovative optimization techniques*

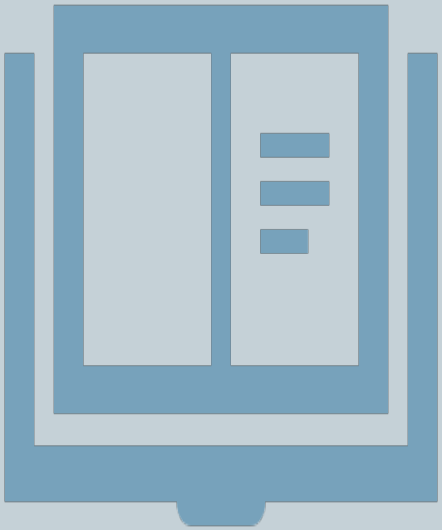

Why are we still interested in binary stars?

Multiplicity is everywhere	*Star formation*
	Population synthesis
Growing sample, better statistics	*Space telescopes*
	Long-term surveys
	Automated analysis
New phenomena	*Accretion disk in the massive CBS*
	Double-periodic variables

“Solving” individual objects

Observations

- RV curves
- Light curves

Detailed modeling

Orbital and stellar parameters

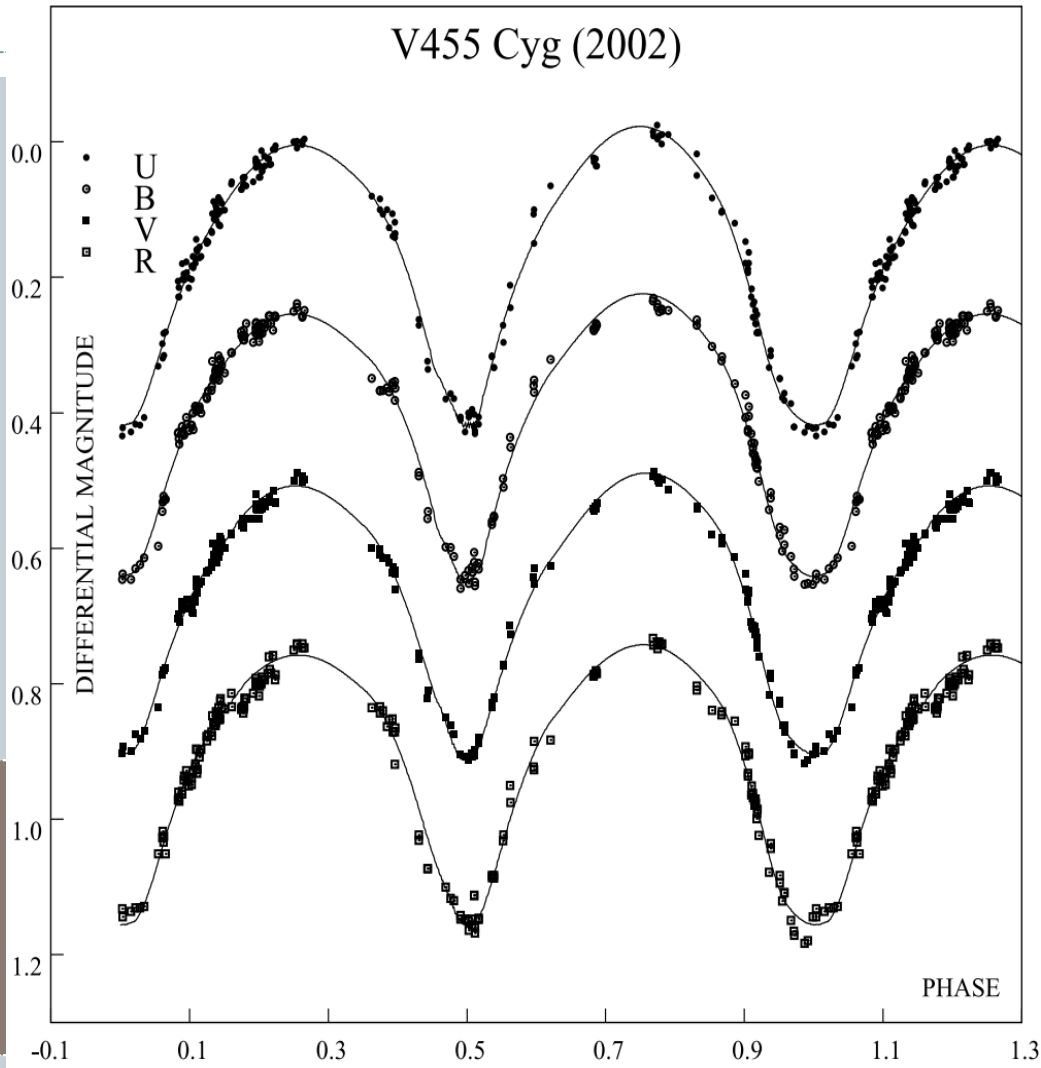

Seasonal light curves of V455 Cyg in the year 2002. From Djurasevic et al., 2012, MNRAS, 420, 308

“Solving” individual objects

Observations

- RV curves
- Light curves

Detailed modeling

Orbital and stellar parameters

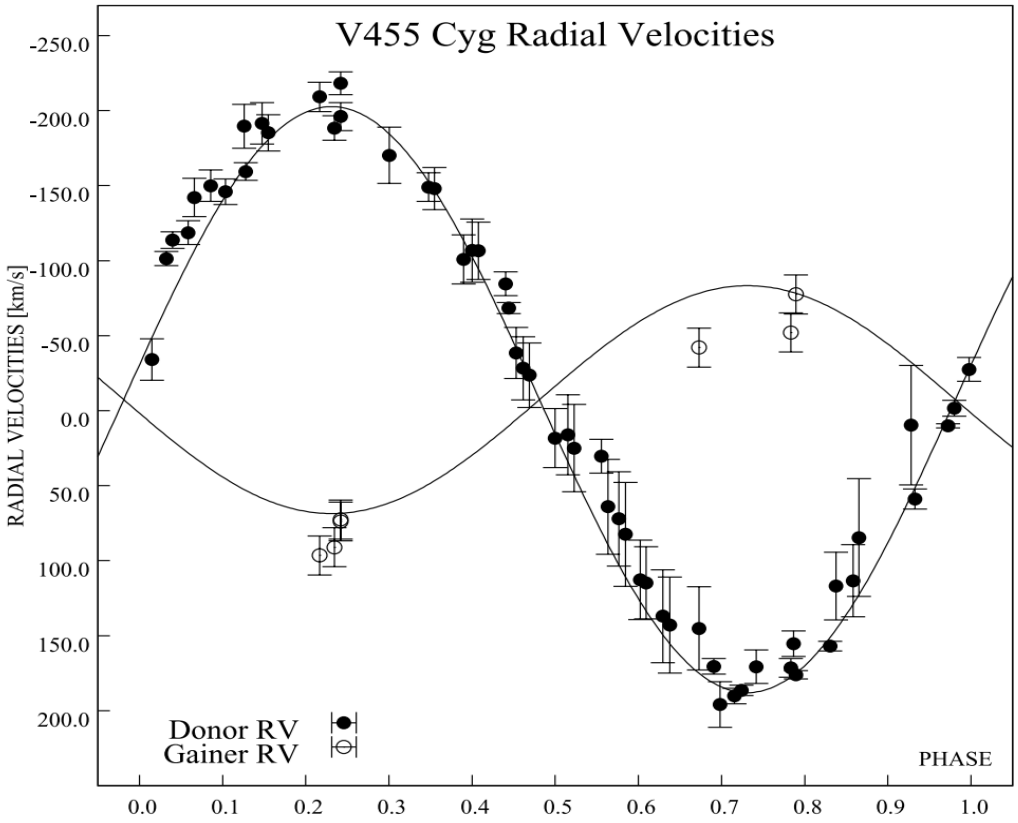

Radial velocity curves of V455 Cyg. From Djurasevic et al., 2012, MNRAS, 420, 308

“Solving” individual objects

Observations
- RV curves
- Light curves

Detailed modeling

Orbital and stellar parameters

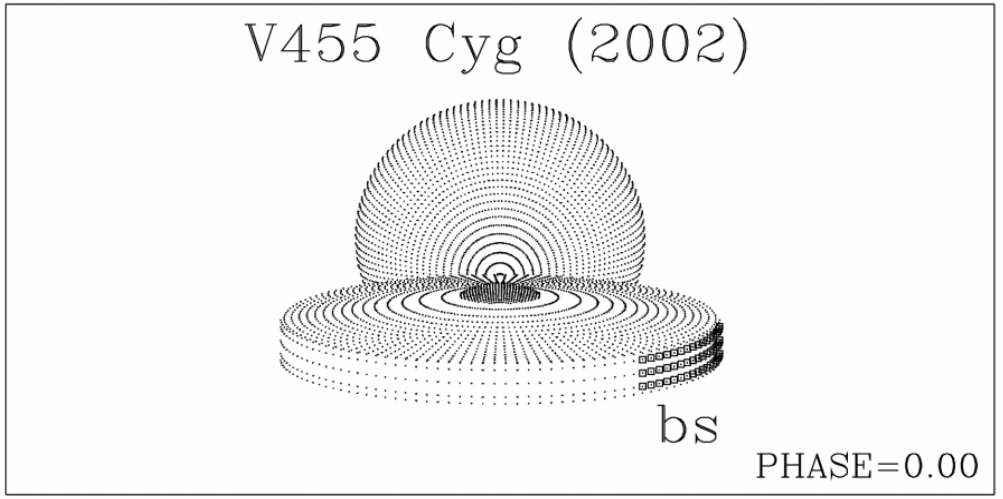

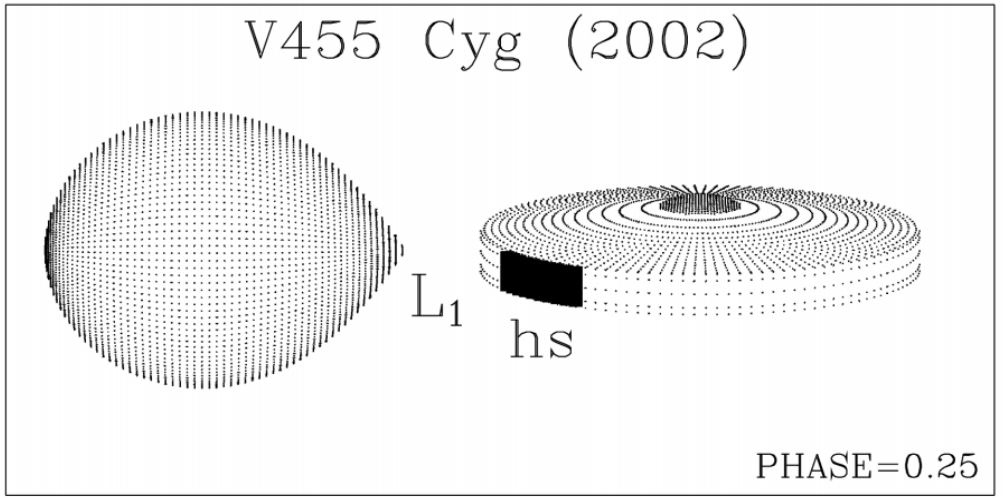

Model of V455 Cyg. From Djurasevic et al., 2012, MNRAS, 420, 308

We develop and maintain our own modeling tools

Binary system modeling software created by G. Đurašević

- Based on Roche geometry
- In constant development
- Accretion disks
- Extremely fast

Infinity

- Reimagined geometrical representation
- Eccentric systems
- Simultaneous fitting of LC and RVC
- Stellar oscillations
- And more...
- ... at the cost of speed.

Future improvements

- Circumstellar structures
- Circumbinary structures
- Synthetic spectra
- Synthetic polarized light curves

High Mass Binaries: Some unresolved problems concerning the light curve modeling

SHORT HISTORY OF THE MODELING THESE VARIABLES

OVER-CONTACT OR THE SYSTEMS WITH ACCRETION DISK ?

A&A 374, 638–645 (2001)
DOI: 10.1051/0004-6361:20010727

Astronomy & Astrophysics

A photometric study of the massive binary RY Sct*

G. Djurašević[1], M. Zakirov[2], M. Eshankulova[3], and S. Erkapić[1]

$$f_{\rm over}[\%] = 100 \cdot (\Omega_{1,2} - \Omega_{\rm i})/(\Omega_{\rm o} - \Omega_{\rm i})$$

The results describe RY Sct's system as an overcontact configuration ($f_{\rm over} \sim 33\%$ – **Hyp. I** and $f_{\rm over} \sim 32\%$ – **Hyp. II**) with a significant temperature difference between the components ($\Delta T = T_{\rm hot} - T_{\rm cool} \sim 3770$ K – **Hyp. I** and $\Delta T = T_{\rm hot} - T_{\rm cool} \sim 4010$ K – **Hyp. II**). These solutions together with a mass ratio of $q = m_{\rm cool}/m_{\rm hot} = 3.3$ suggest a significant mass and energy transfer from the less-massive (hotter) secondary onto the more-massive (cooler) primary. The hot area on the cooler star, near the neck region, can be taken as a consequence of this mass and energy exchange between the components through the connecting neck of the common envelope. Apparently, another hot area (near the external Lagrange point L_3) is the zone of an intensive mass outflow from the system. Without this hot region we have a poorer fit again. This mechanism, together with mass loss through stellar wind, could be responsible for the existing nebula around RY Sct.

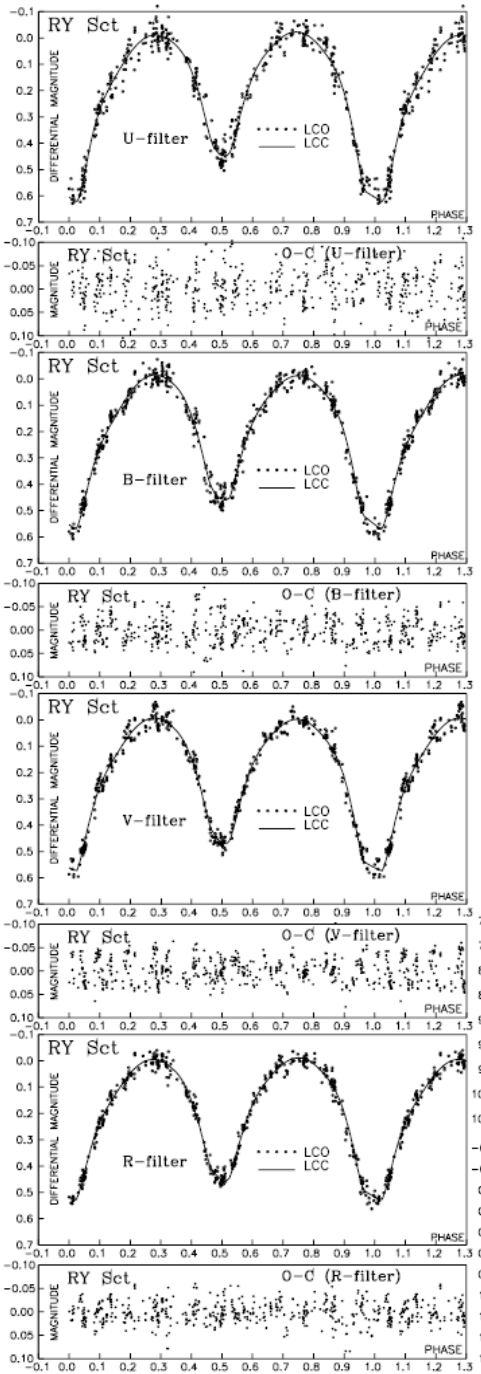

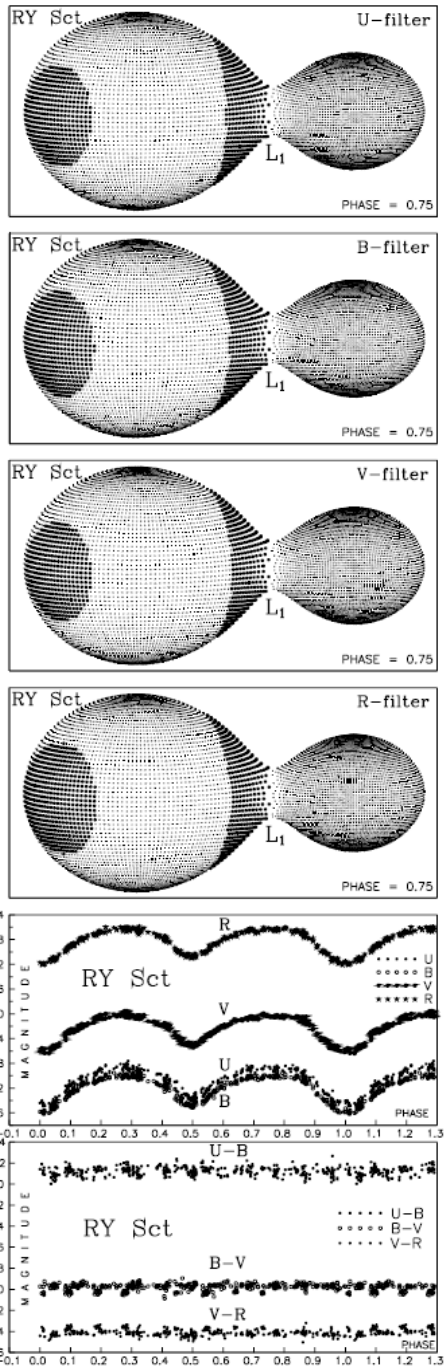

The Astronomical Journal, 136:767–772, 2008 August

ACCRETION DISK IN THE MASSIVE BINARY RY SCUTI

G. Djurašević, I. Vince, O. Atanacković[1]

$$T(r) = T_{\rm d}\left(\frac{R_{\rm d}}{r}\right)^{a_T}\left(1-\sqrt{\frac{R_*}{r}}\right)^{\frac{1}{4}}\left(1-\sqrt{\frac{R_*}{R_{\rm d}}}\right)^{-\frac{1}{4}}, \quad (1)$$

$$T(r) = T_{\rm d}\left(\frac{R_{\rm d}}{r}\right)^{a_T}, \quad (2)$$

$$T(r) = T_{\rm d} + (T_* - T_{\rm d})\left[1-\left(\frac{r-R_*}{R_{\rm d}-R_*}\right)\right]^{a_T}, \quad (3)$$

$$T(r) = T_{\rm d} + (T_* - T_{\rm d})\left[1-\left(\frac{r-R_*}{R_{\rm d}-R_*}\right)^{a_T}\right]. \quad (4)$$

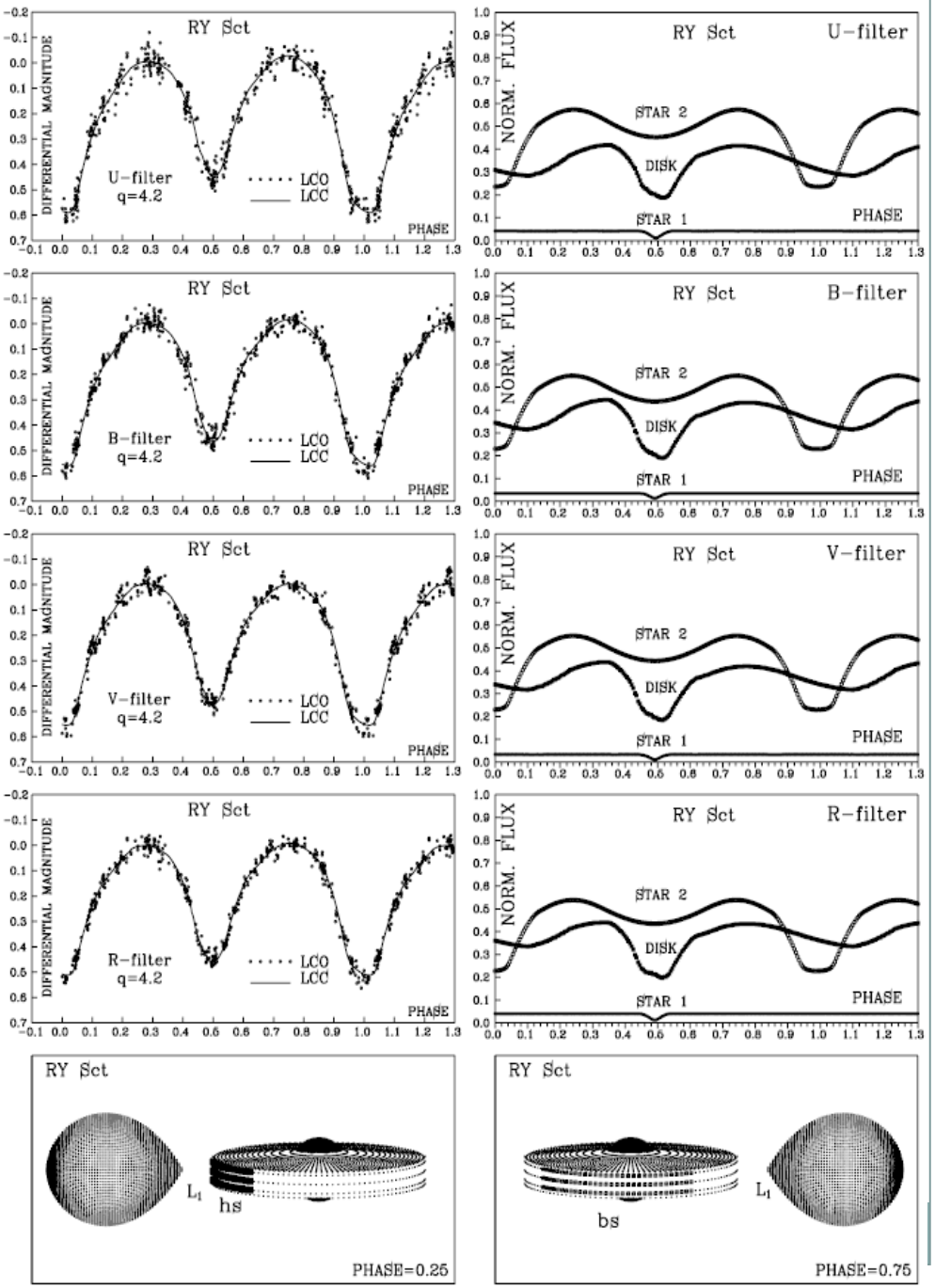

Mon. Not. R. Astron. Soc. 420, 3081–3090 (2012) doi:10.1111/j.1365-2966.2011.20208.x

A study of the interacting binary system V455 Cygni

G. Djurašević,[1,2]★ I. Vince,[1] I. I. Antokhin,[3] N. I. Shatsky,[3] A. Cséki,[1] M. Zakirov[4] and M. Eshankulova[5]

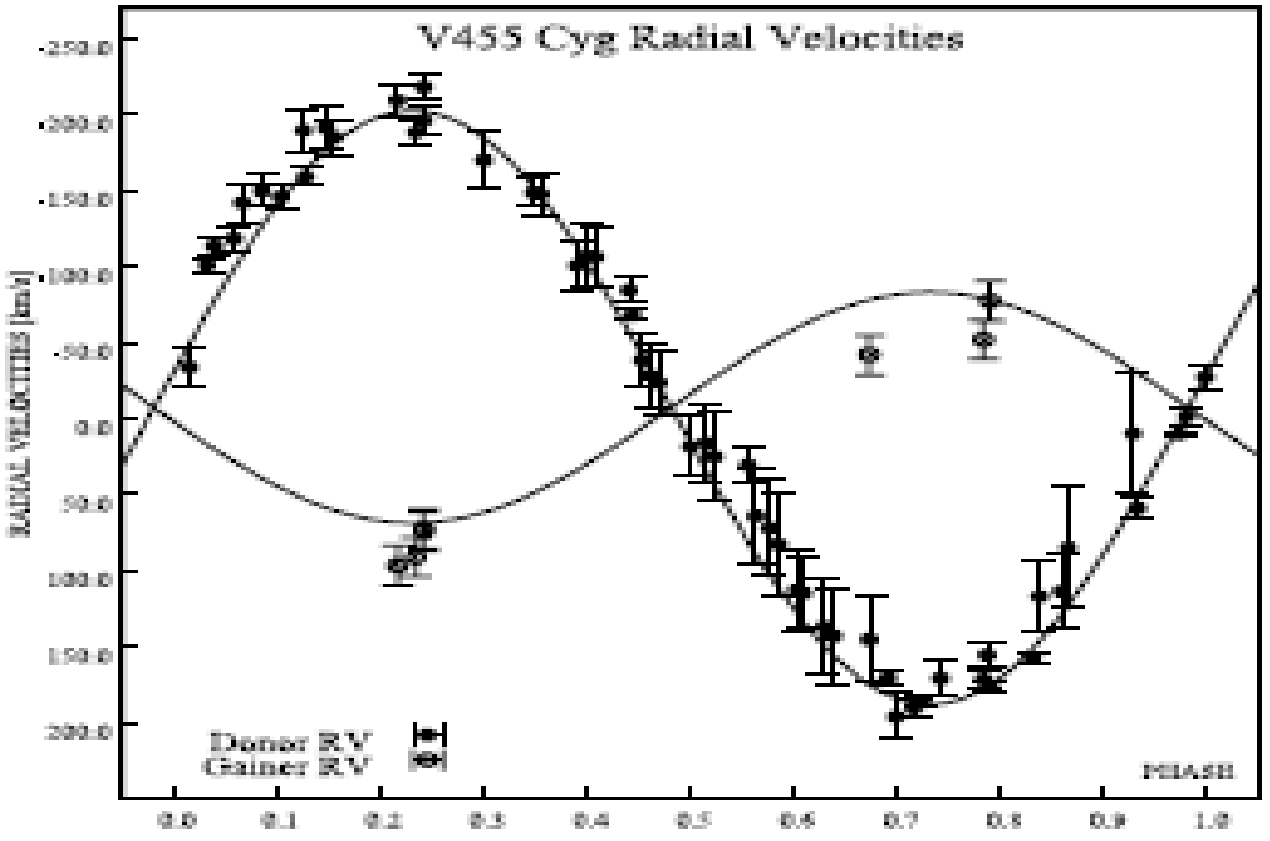

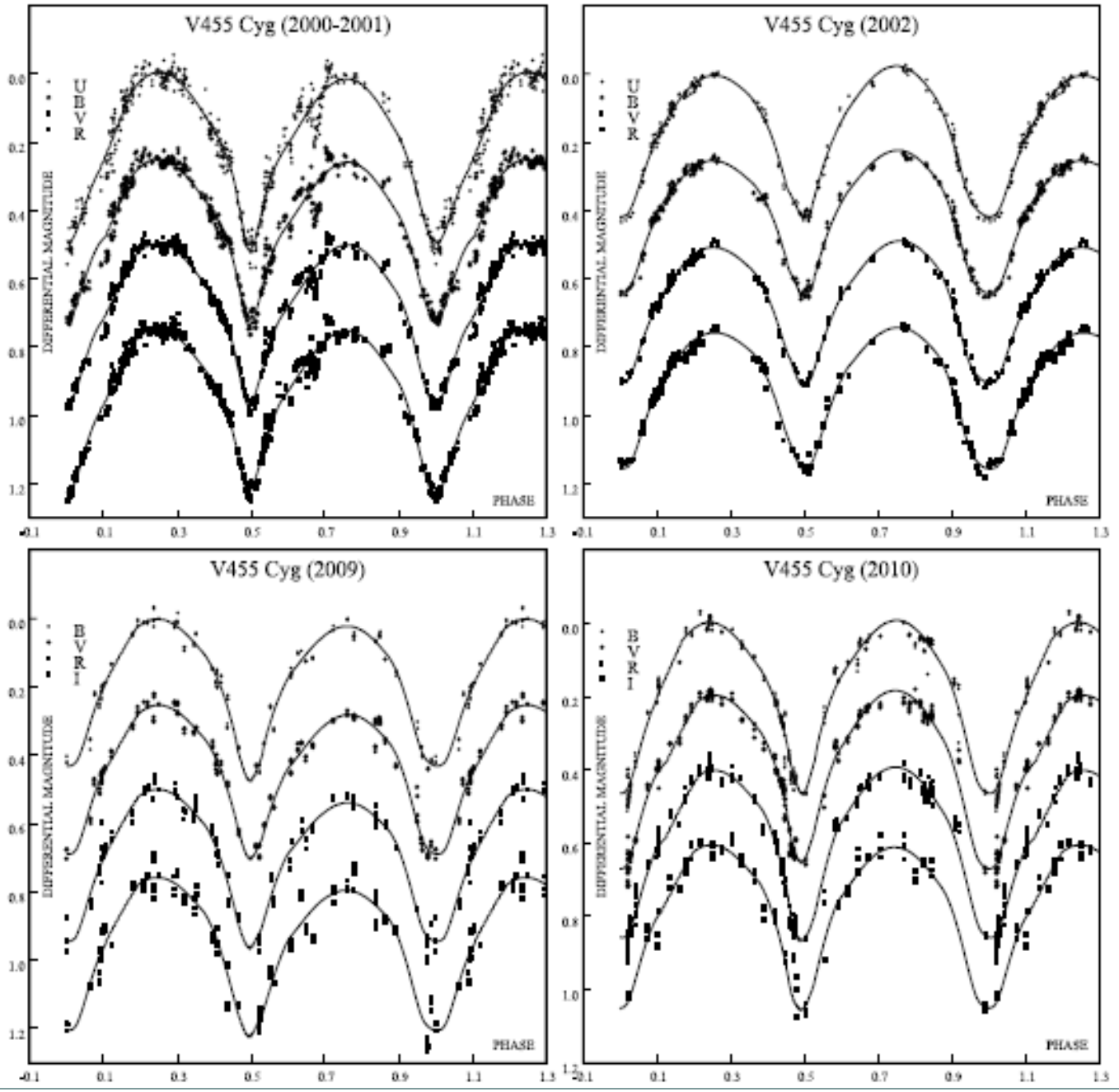
V455 Cyg (2000-2001)
U
B
V
R
DIFFERENTIAL MAGNITUDE
PHASE
V455 Cyg (2002)
U
B
V
R
DIFFERENTIAL MAGNITUDE
PHASE
V455 Cyg (2009)
B
V
R
I
DIFFERENTIAL MAGNITUDE
PHASE
V455 Cyg (2010)
B
V
R
I
DIFFERENTIAL MAGNITUDE
PHASE

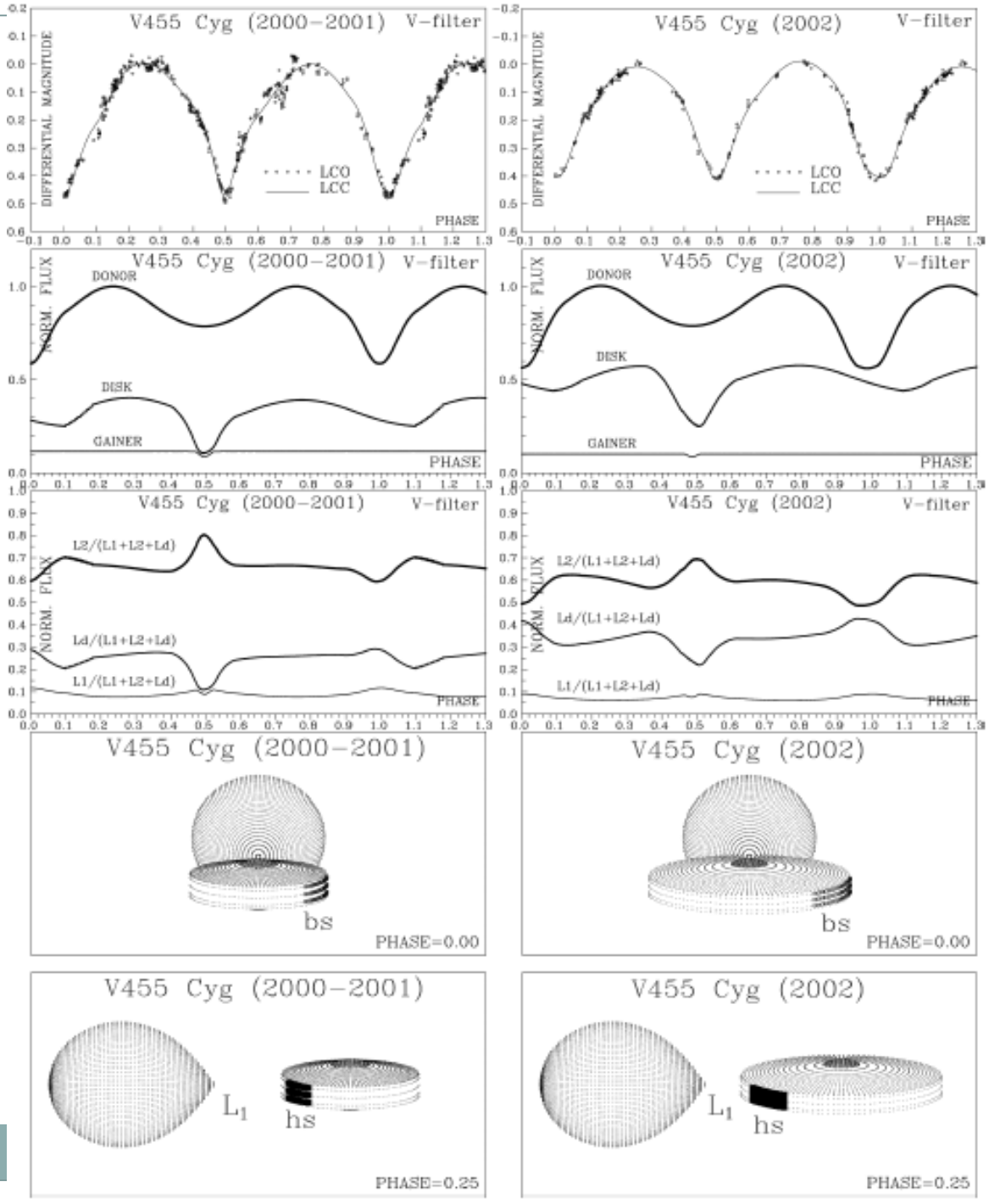
V455 Cyg (2000−2001) V-filter
DIFFERENTIAL MAGNITUDE
LCO
LCC
PHASE
V455 Cyg (2002) V-filter
DIFFERENTIAL MAGNITUDE
LCO
LCC
PHASE
V455 Cyg (2000−2001) V-filter
NORM. FLUX
DONOR
DISK
GAINER
PHASE
V455 Cyg (2002) V-filter
NORM. FLUX
DONOR
DISK
GAINER
PHASE
V455 Cyg (2000−2001) V-filter
NORM. FLUX
L2/(L1+L2+Ld)
Ld/(L1+L2+Ld)
L1/(L1+L2+Ld)
PHASE
V455 Cyg (2002) V-filter
NORM. FLUX
L2/(L1+L2+Ld)
Ld/(L1+L2+Ld)
L1/(L1+L2+Ld)
PHASE
V455 Cyg (2000−2001)
bs
PHASE=0.00
V455 Cyg (2002)
bs
PHASE=0.00
V455 Cyg (2000−2001)
L1
hs
PHASE=0.25
V455 Cyg (2002)
L1
hs
PHASE=0.25

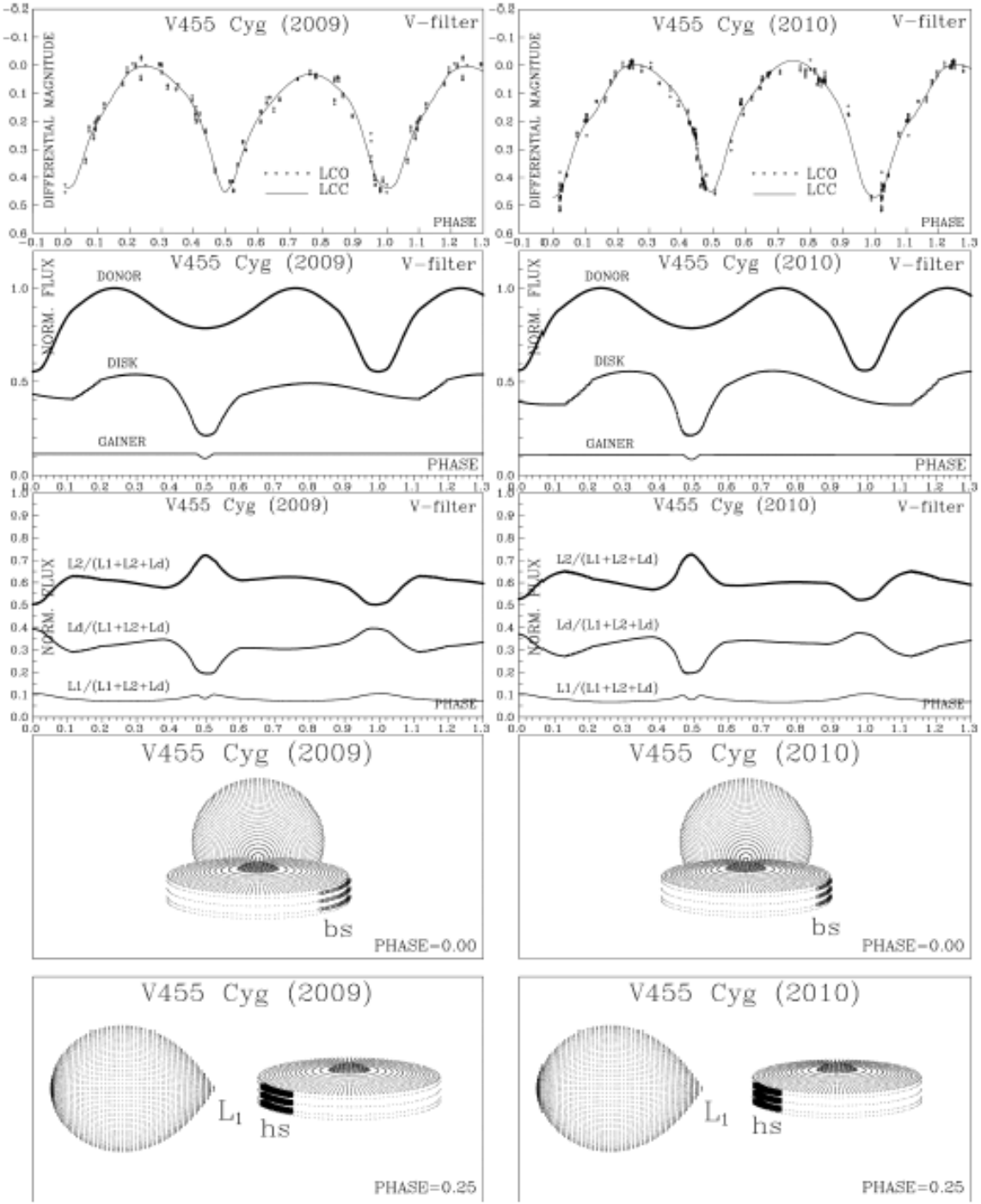

Figure 5. The same as in Fig. 2, but for 2009 and 2010 seasonal photometric observations.

Mon. Not. R. Astron. Soc. **396,** 1553–1558 (2009) doi:10.11

Accretion disc in the massive V448 Cygni system

G. Djurašević,[1,2★] I. Vince,[1] T. S. Khruzina[3] and E. Rovithis-Livaniou[4]

$$T(r) = T_{\rm d} + (T_* - T_{\rm d}) \left[1 - \left(\frac{r - R_*}{R_{\rm d} - R_*} \right) \right]^{\varepsilon_T}$$

The temperature distribution along disk radius

Table 1. Results of the analysis of V448 Cygni light curves obtained by solving the inverse problem for the Roche model with an accretion disc around the more massive (hotter) component.

Quantity	*U* filter	*B* filter	*V* filter	Mean
n	543	544	541	
$\Sigma(O-C)^2$	1.3820	0.4833	0.5626	
σ_{rms}	0.0502	0.0298	0.0322	
i (°)	87.9	88.0	87.8	87.9 ± 0.5
F_d	0.97	0.97	0.97	0.97 ± 0.02
T_d(K)	26 320	23 700	24 150	$24\,700 \pm 1600$
$d_e(a_{orb})$	0.086	0.085	0.085	0.085 ± 0.009
$d_c(a_{orb})$	0.06	0.06	0.06	0.06 ± 0.02
a_T	1.84	1.81	1.82	1.8 ± 0.2
F_h	0.384	0.385	0.385	0.385 ± 0.008
T_c(K)	20 350	20 410	20 260	$20\,340 \pm 150$
$A_{HS} = T_{HS}/T_d$	1.20	1.12	1.14	1.15 ± 0.08
θ_{HS}(°)	18.7	19.3	18.1	18.7 ± 0.9
λ_{HS}(°)	327.5	327.8	327.3	327.5 ± 2.1
θ_{rad}(°)	−24.8	−22.8	−19.3	-22.3 ± 5.7
$A_{BS} = T_{BS}/T_d$	1.32	1.30	1.32	1.31 ± 0.06
θ_{BS}(°)	45.6	43.7	45.9	45.1 ± 3.0
λ_{BS}(°)	112.2	109.9	105.8	109.3 ± 4.5
Ω_h	6.96	6.95	6.95	6.95 ± 0.03
Ω_c	2.98	2.98	2.98	2.98 ± 0.02
$\mathcal{M}_h(\mathcal{M}_\odot)$	24.7	24.7	24.7	24.7 ± 0.7
$\mathcal{M}_c(\mathcal{M}_\odot)$	13.7	13.7	13.7	13.7 ± 0.7
$\mathcal{R}_h(R_\odot)$	7.7	7.8	7.8	7.8 ± 0.2
$\mathcal{R}_c(R_\odot)$	16.3	16.3	16.3	16.3 ± 0.3
$\log g_h$	4.05	4.05	4.05	4.05 ± 0.03
$\log g_c$	3.15	3.15	3.15	3.15 ± 0.03
M^h_{bol}	−6.88	−6.89	−6.88	-6.88 ± 0.08
M^c_{bol}	−6.74	−6.75	−6.72	-6.74 ± 0.08
$a_{orb}(R_\odot)$	49.5	49.5	49.5	49.5 ± 0.6
$\mathcal{R}_d(R_\odot)$	20.6	20.6	20.7	20.6 ± 0.5
$d_e(R_\odot)$	4.22	4.22	4.23	4.2 ± 0.3
$d_c(R_\odot)$	3.10	3.13	3.11	3.1 ± 0.3

Fixed parameters: $q = \mathcal{M}_c/\mathcal{M}_h = 0.555$ – mass ratio of the components; $T_h = 30\,490$ K – temperature of the more massive (hotter) star; $F_c = 1.0$ – filling factor for the critical Roche lobe of the cooler (less massive) star; $f_h = f_c = 1.00$ – non-synchronous rotation coefficients of the components; $\beta_{h,c} = 0.25$ – gravity-darkening coefficients of the components and $A_{h,c} = 1.0$ – albedo coefficients of the components.

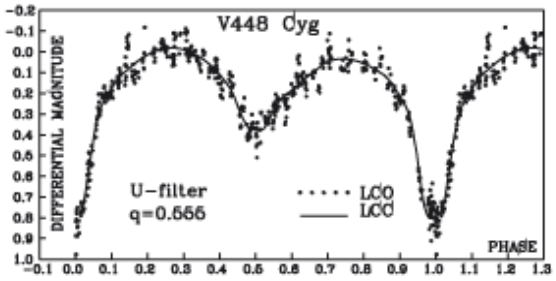

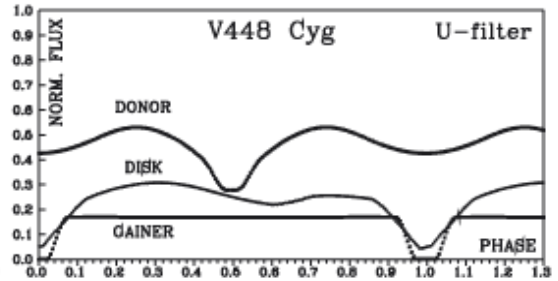

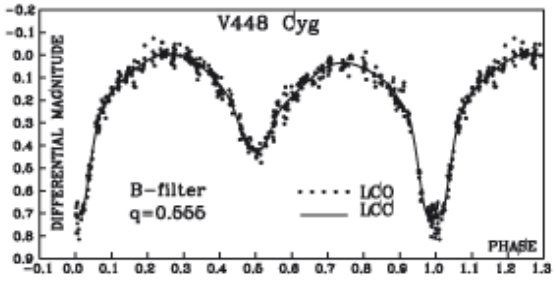

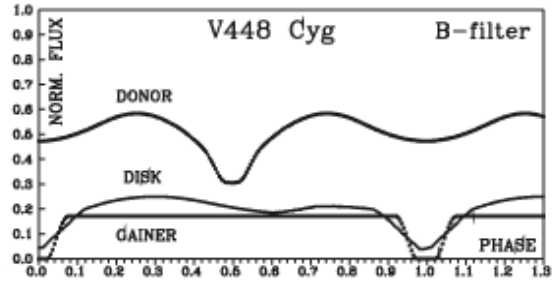

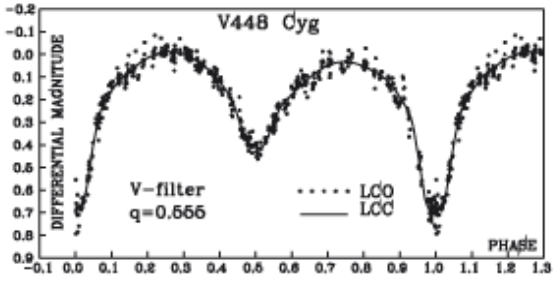

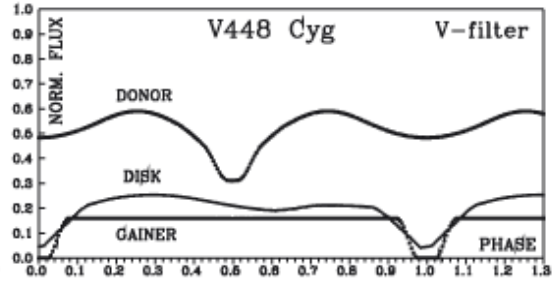

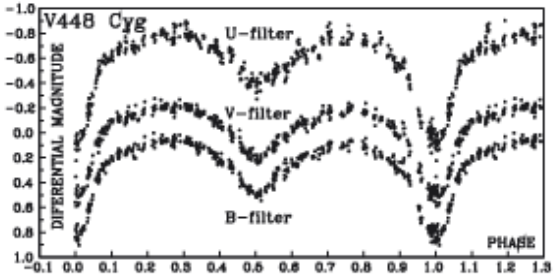

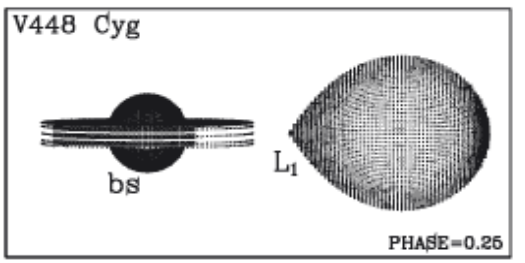

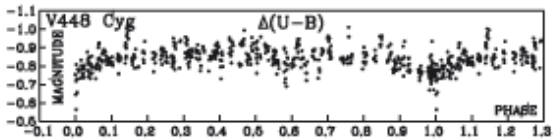

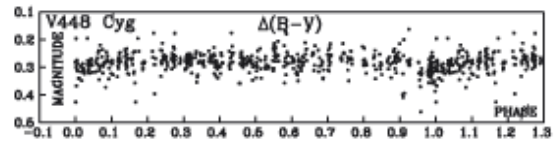

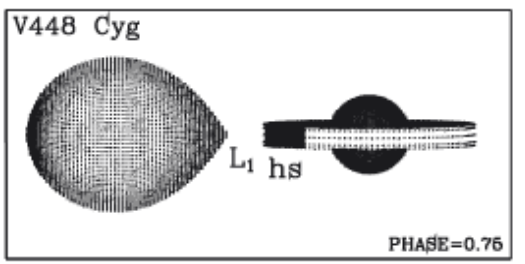

AU Mon

Ултра-прецизна фотометрија са сателитског телескопа CoRoT

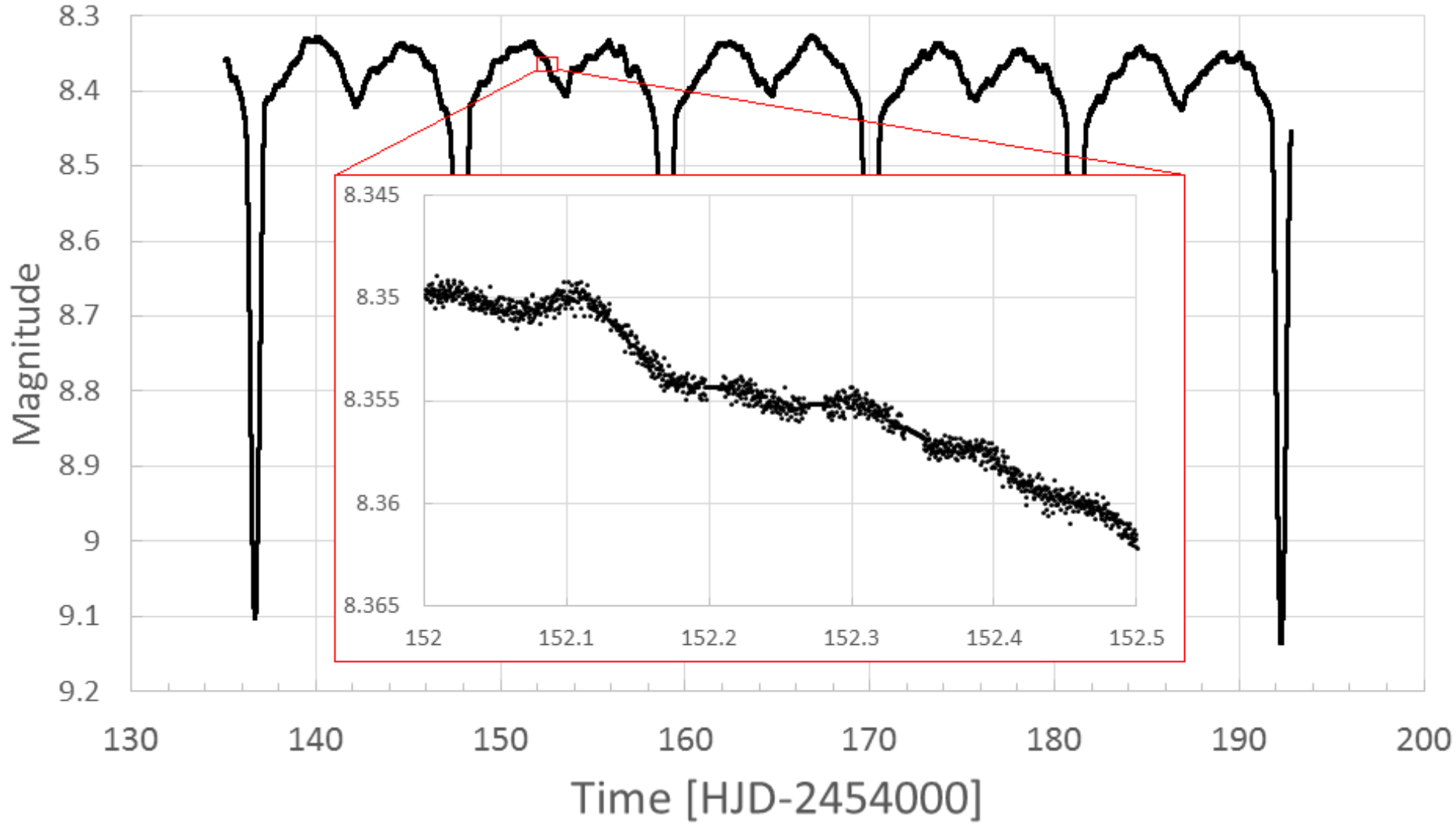

AU Mon

Desmet et al. 2010, MNRAS, 401, 418

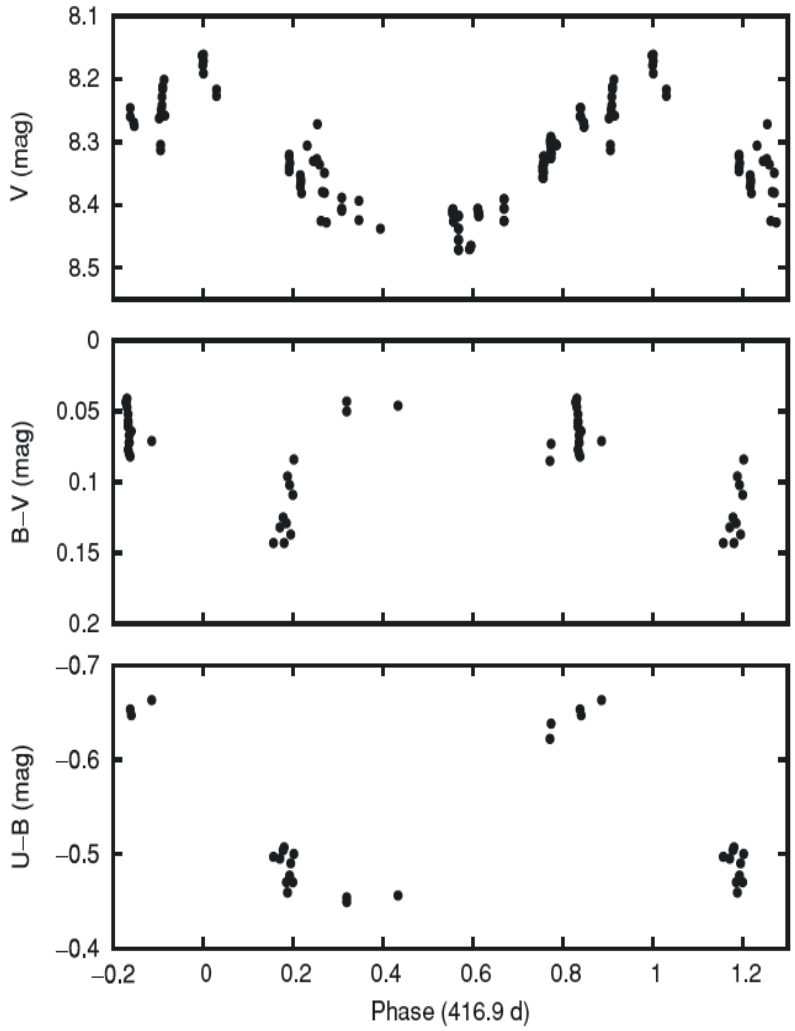

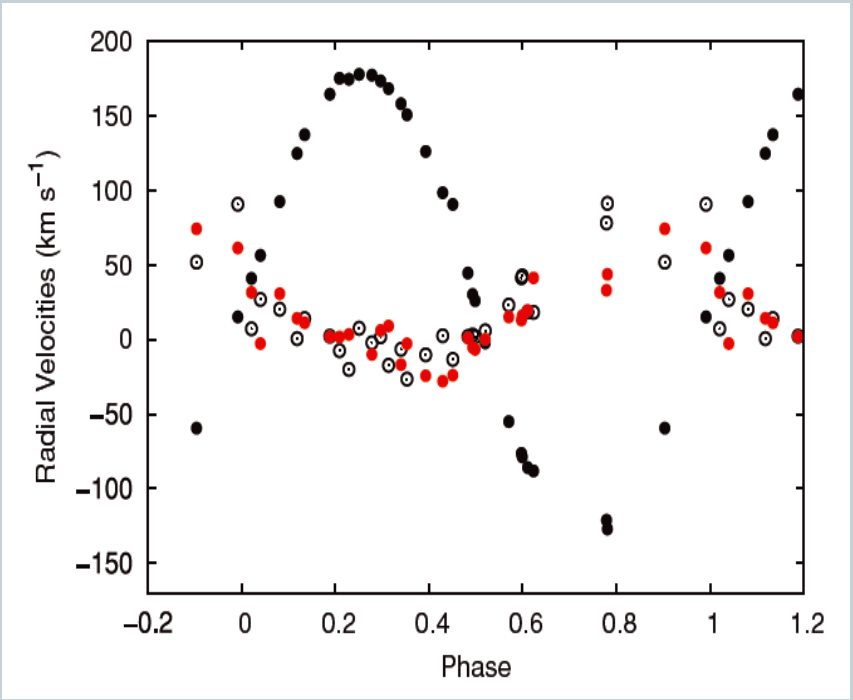

AU Mon

Đurašević, Latković, Vince & Čeki 2010, MNRAS, 409, 329

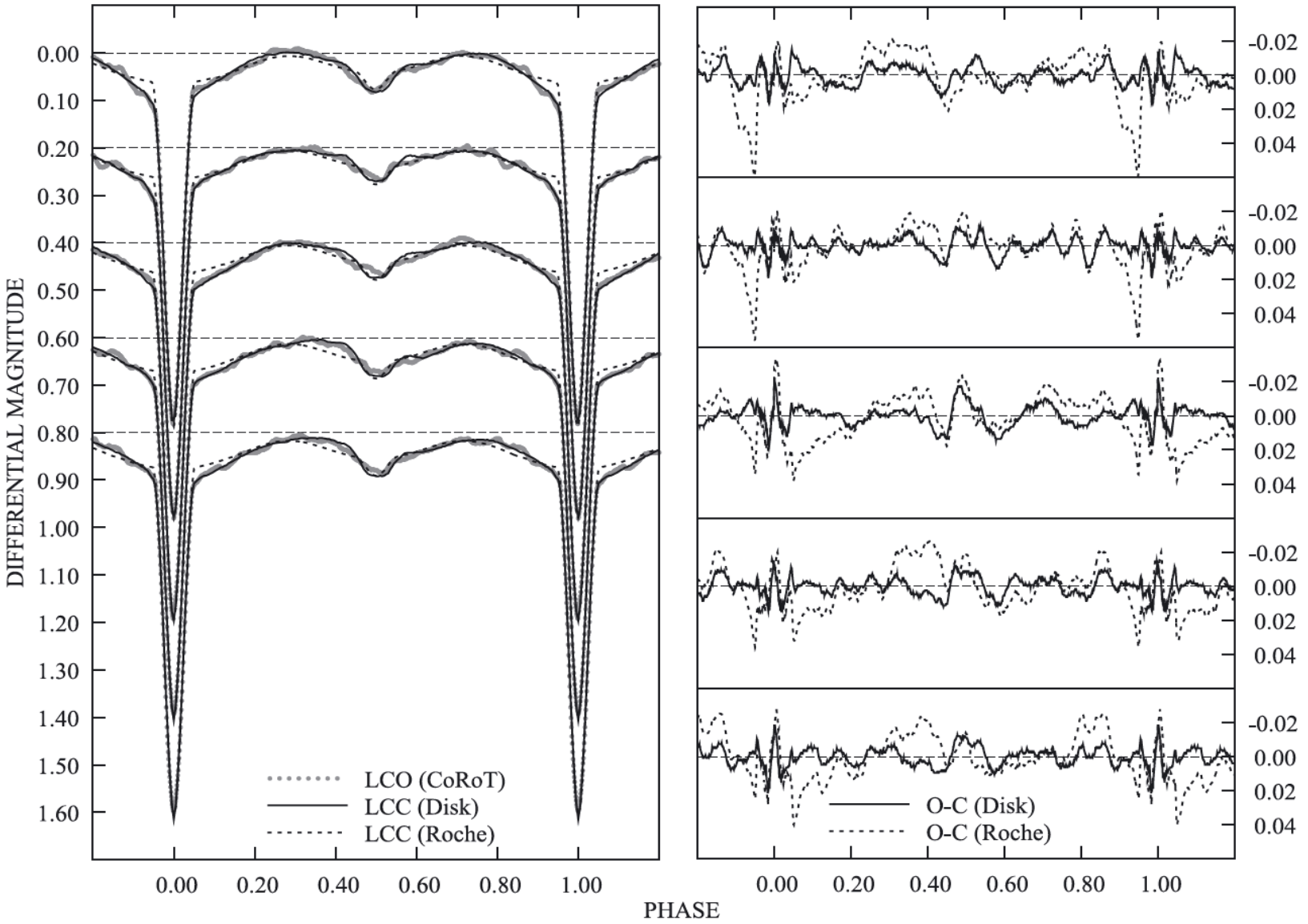

AU Mon

Đurašević, Latković, Vince & Čeki 2010, MNRAS, 409, 329

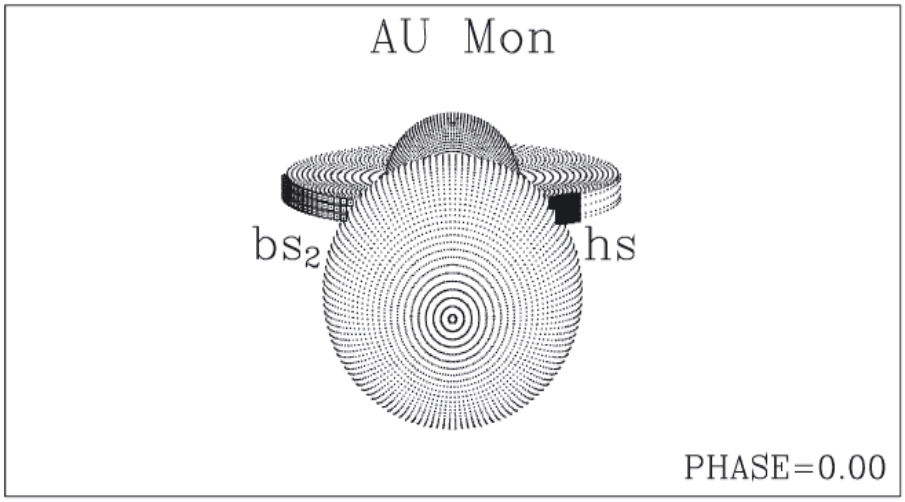

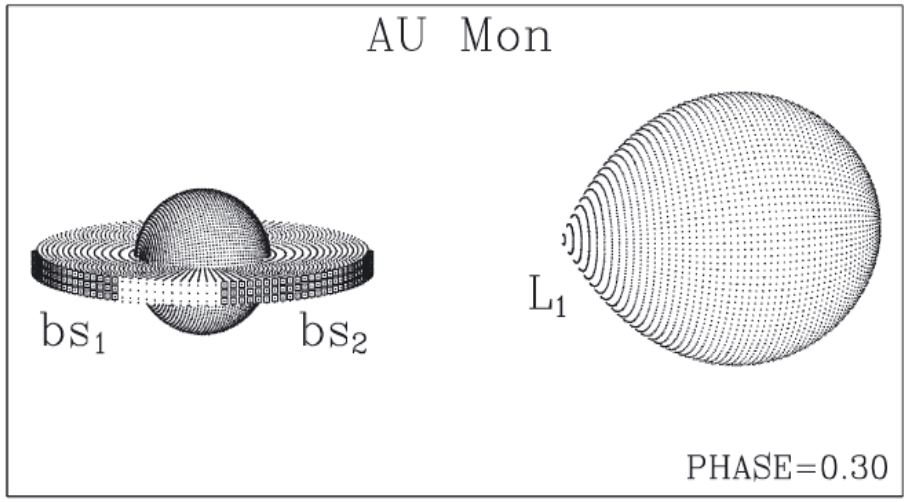

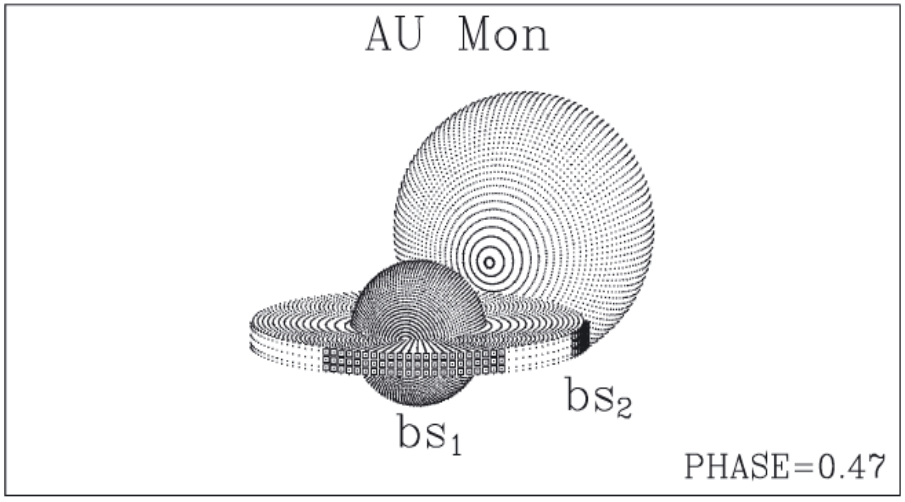

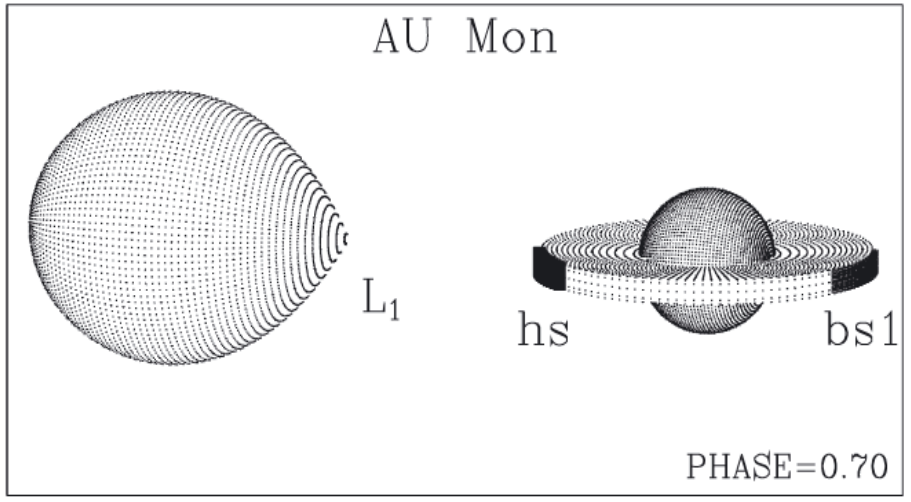

Discovery of the Double-periodic variables

Mennickent et al. 2003, A&A, 399, L47

- OGLE II и MACHO
- Група плавих објеката у Магелановим Облацима са две врсте фотометријске променљивости:
  - Кратка периодична променљивост амплитуде $\Delta I \approx 0.05\, mag$ и периода $4^d < P < 16^d$
  - Дуга периодична променљивост амплитуде $\Delta I \approx 0.2\, mag$ и периода $150^d < P < 1000^d$
- Кратка периодична променљивост личи на криве сјаја типичне за двојне звезде Алголовог типа
- Целобројни однос између кратког и дугог периода

Double-periodic variables

Two photometric periodicities

- Short cycle (orbital period): P_o
- Long cycle (unknown): P_L
- $P_L \approx 33 \times P_O$

Semidetached binaries in midst of mass transfer

Census

Nature of long cycle ?

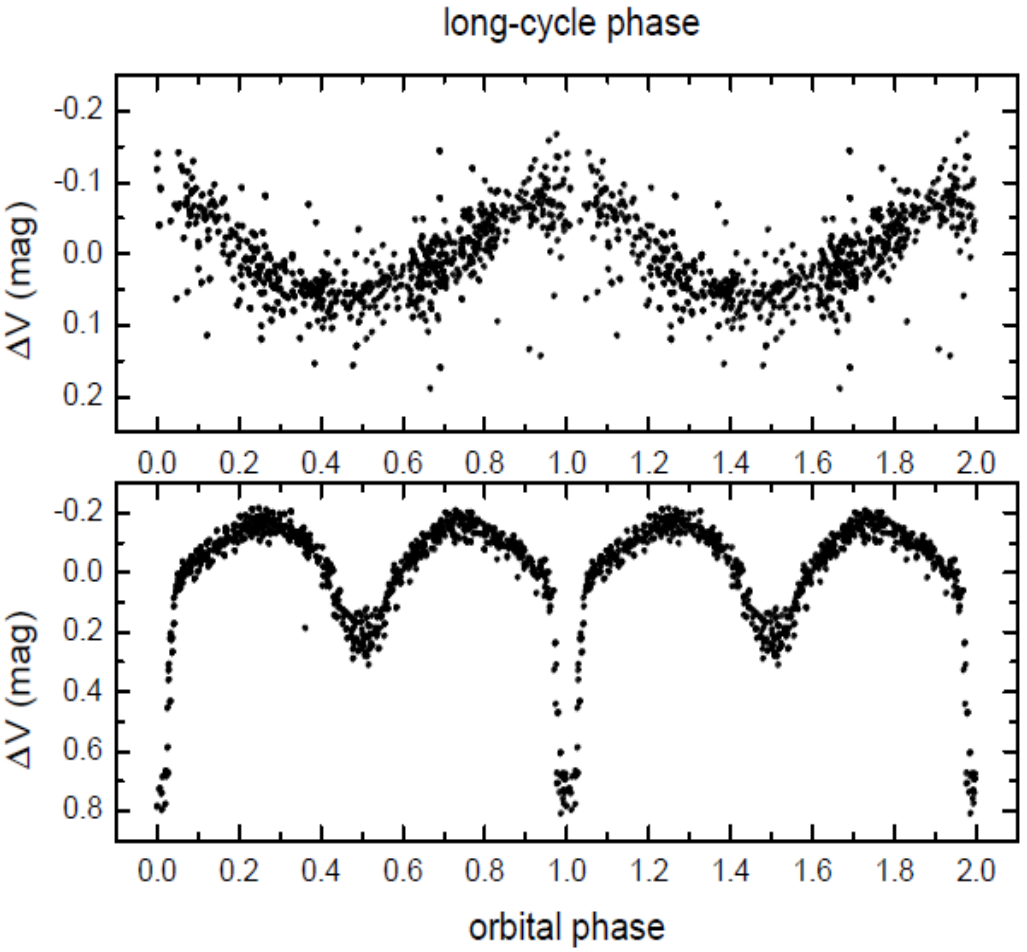

Disentangled light curve of V495 Cen. Orbital Period is P~33d and long cycle is LP~1283d. From Mennickent & Rosales, 2014, IBVS 6116,1

Double-periodic variables

Two photometric periodicities

- Short cycle (orbital period): P_o
- Long cycle (unknown): P_L
- $P_L \approx 33 \times P_O$

Semidetached binaries in midst of mass transfer

Census

Nature of long cycle ?

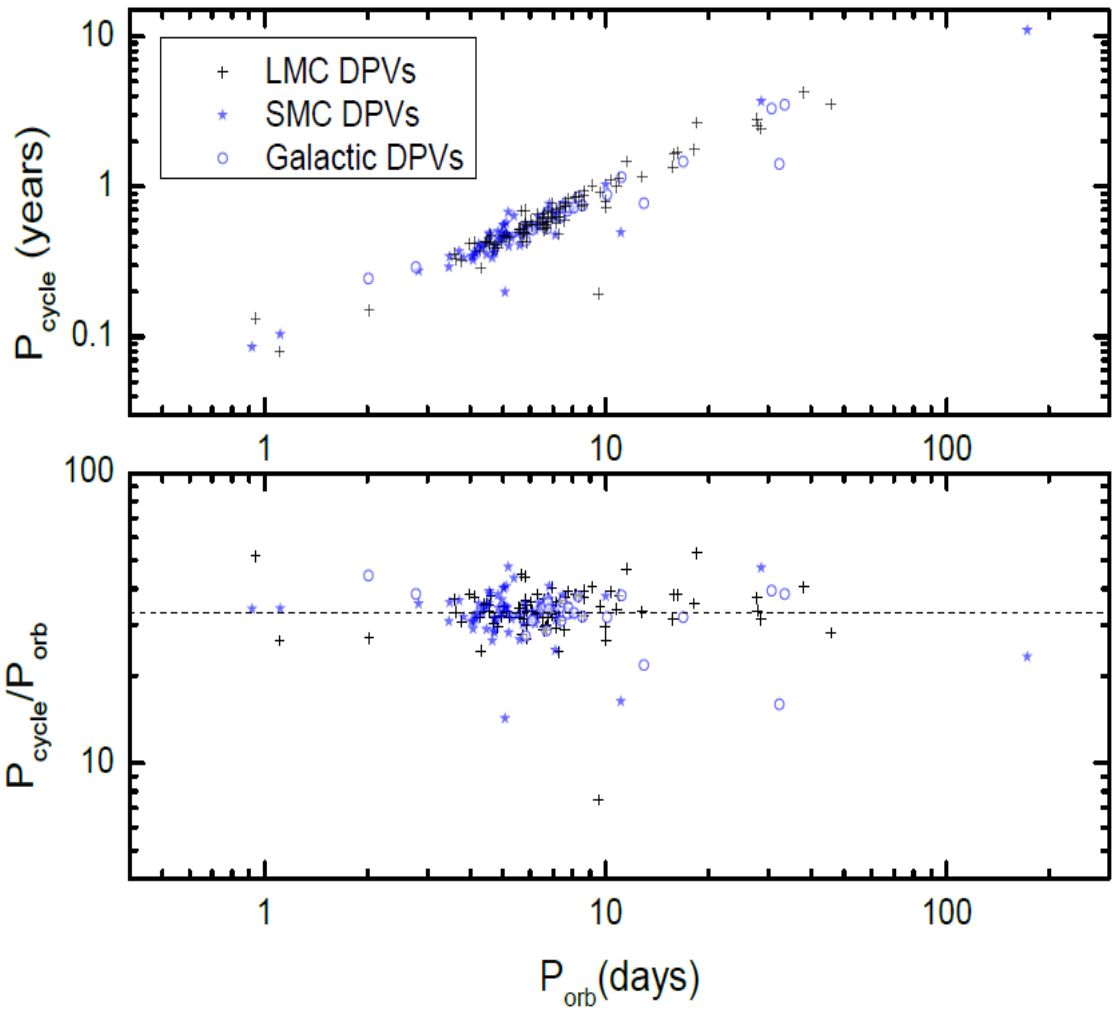

Orbital periods and long cycles for the entire DPV sample. From Mennickent, 2017, Ser AJ 194, 1

Double-periodic variables

Two photometric periodicities

Semidetached binaries in midst of mass transfer

- Intermediate to high mass
- Low mass ratio
- Accretion disk
- Hot spot + winds/jets

Census

Nature of long cycle

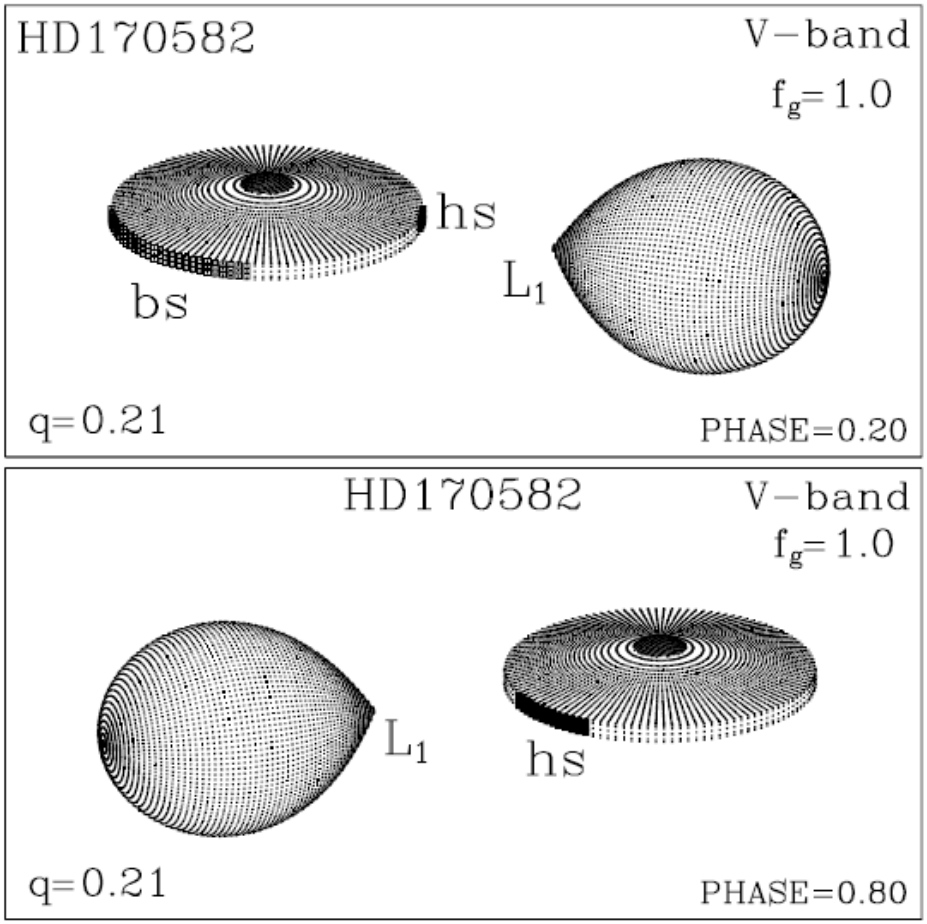

Morphology of DPV HD 170582. From Mennickent, Djurasevic et al., 2015, MNRAS 448, 1137

Double-periodic variables

- Two photometric periodicities
- Semidetached binaries in midst of mass transfer
- Census
  - 137 in LMC + 55 in SMC
  - 21 in Milky Way
  - ≈ 5% of all Algols
- Nature of long cycle ... ?

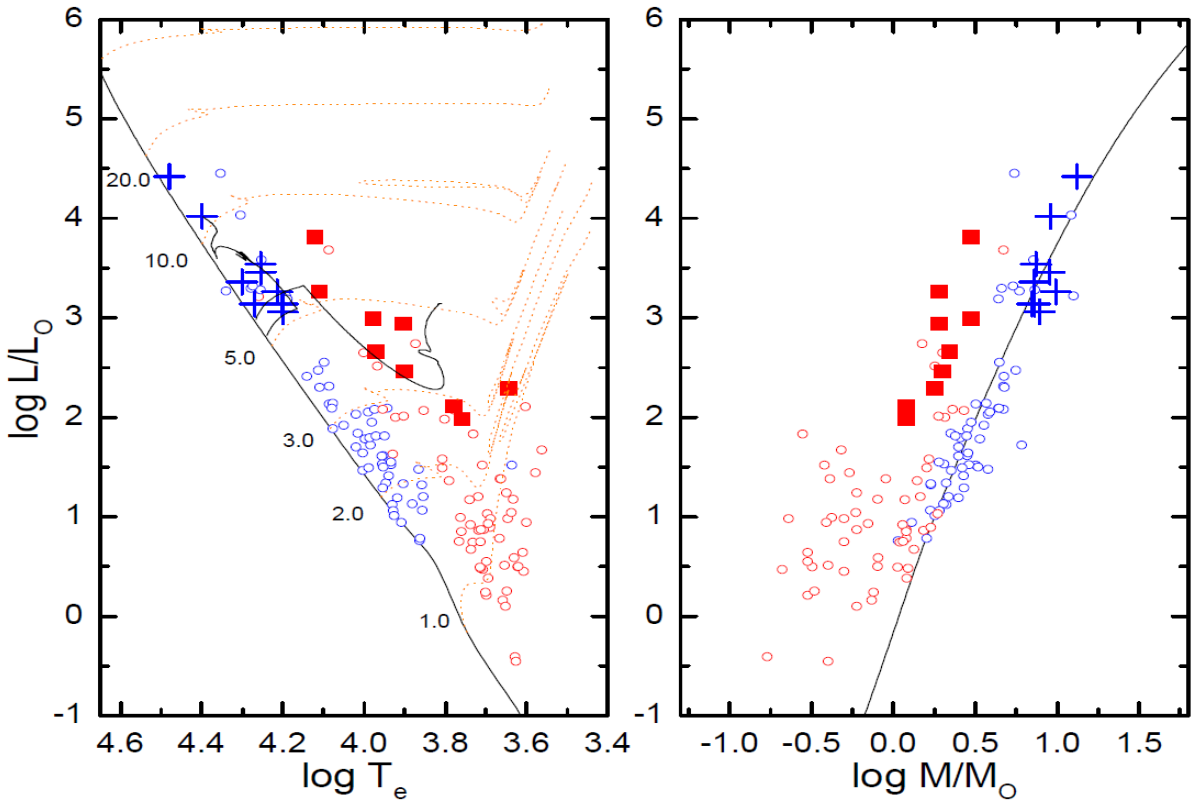

Comparison of galactic Algols and DPVs on HR and ML diagram. From Mennickent, 2017, SerAJ 194, 1

Double-periodic variables

- Two photometric periodicities
- Semidetached binaries in midst of mass transfer
- Census
- Nature of long cycle

- Magnetically active donor
- Applegate mechanism
- Variable oblateness
- Variable accretion rate
- ? .....

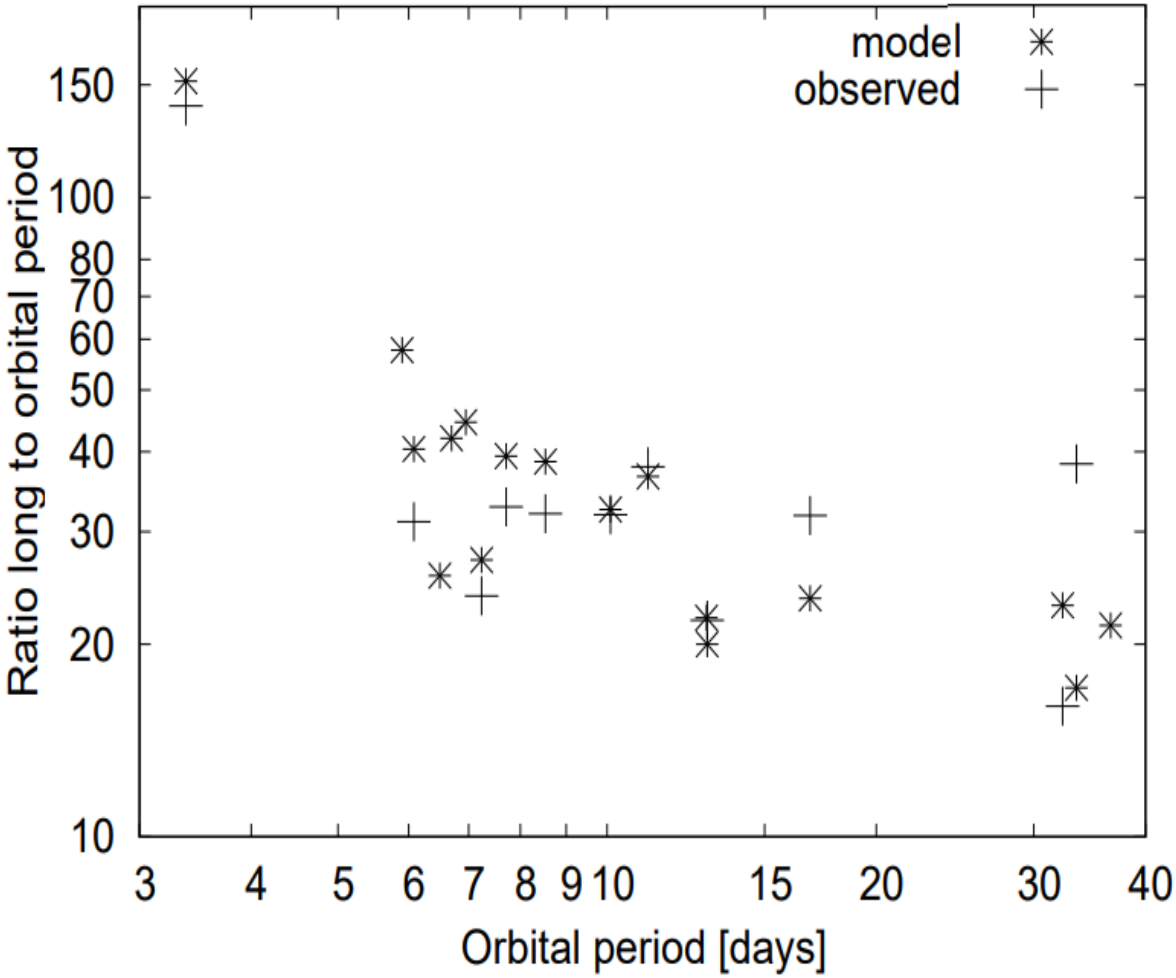

Ratio of long to short cycle vs. short cycle from dynamo model. From Schleicher & Mennickent, 2017, A&A, 602, A109

Mon. Not. R. Astron. Soc. 421, 862–871 (2012) doi:10.1111/j.1365-2966.2011.20363.x

The evolution stage and massive disc of the interacting binary V 393 Scorpii

R. E. Mennickent,[1]★ G. Djurašević,[2,3] Z. Kołaczkowski[1,4] and G. Michalska[1,4]

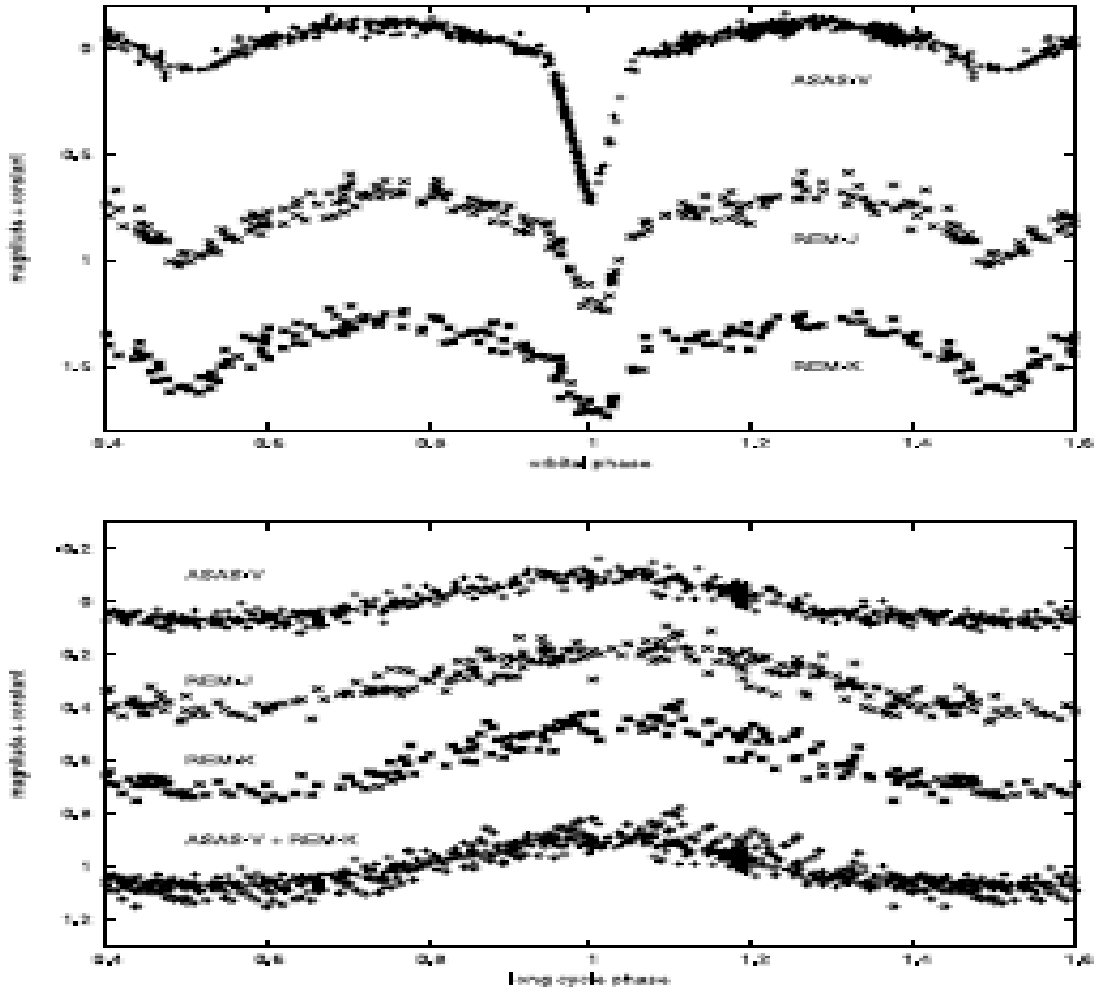

Figure 1. Orbital light curve (up) and long-cycle light curve (down) of V 393 Scorpii at three bandpasses. Ephemeris is given in the text. In the lower light curve circles represent REM–*K* and pluses ASAS–*V* data.

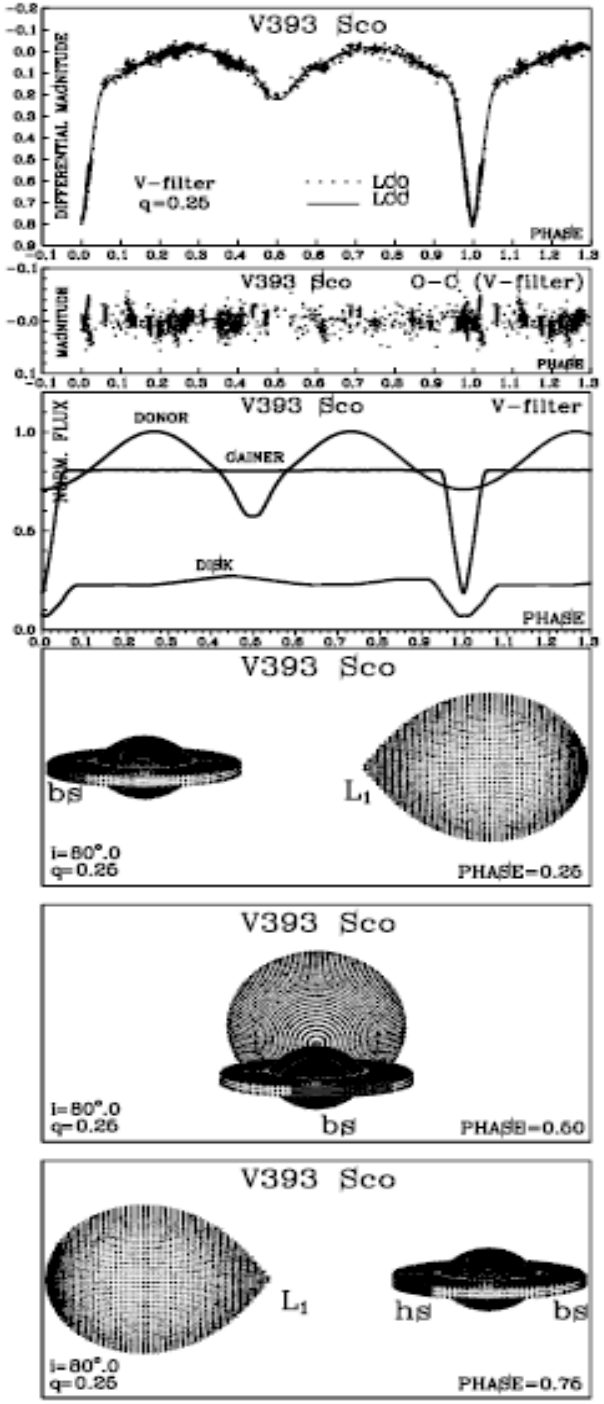

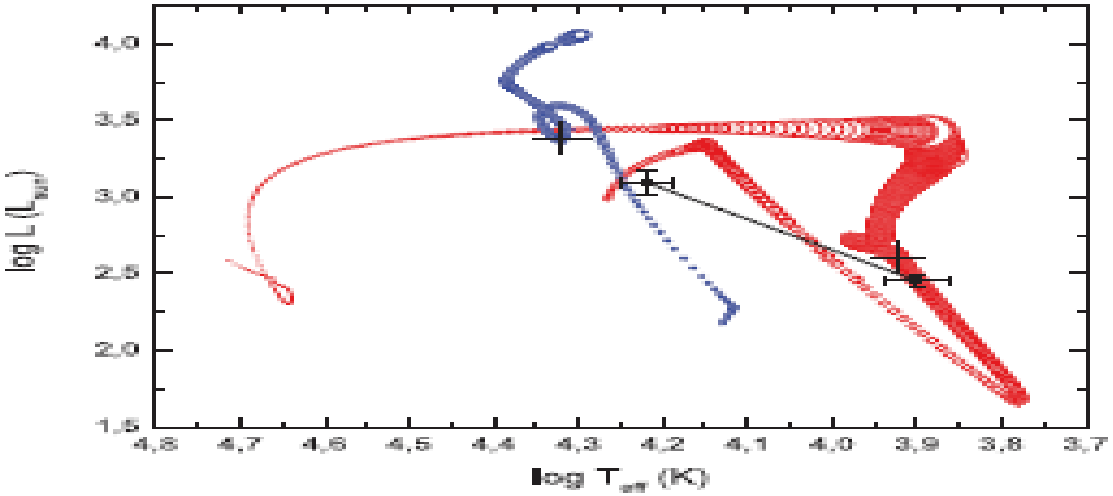

Figure 4. Evolutionary tracks for the binary star model from van Rensbergen et al. (2008) that best fit the data. Donor (right track) and gainer (left track) evolutionary paths are shown, along with the observations for V 393 Scorpii (with error bars and connecting line). The best fit is reached at the time corresponding to the model indicated by large crosses, that is characterized in Table 3. The mismatch for the primary is discussed in the text. Stellar sizes are proportional to the circle diameters.

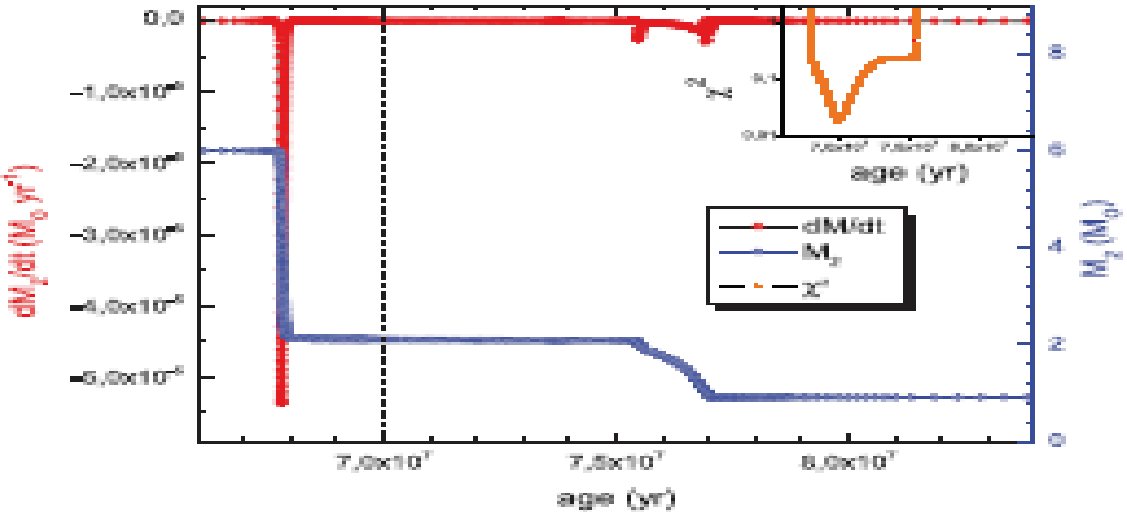

Figure 5. $\dot{M}_2$ (upper curve) and M_2 for the best evolutionary model. The vertical dashed line indicates the position for the best model. χ^2 is shown in the inset graph.

Mon. Not. R. Astron. Soc. 427, 607–624 (2012) doi:10.1111/j.1365-2966.2012.21309.x

A cyclic bipolar wind in the interacting binary V 393 Scorpii

R. E. Mennickent,[1,*†] Z. Kołaczkowski,[1,2] G. Djurasevic,[3,4] E. Niemczura,[2] M. Diaz,[5] M. Curé,[6] I. Araya[6] and G. J. Peters[7]

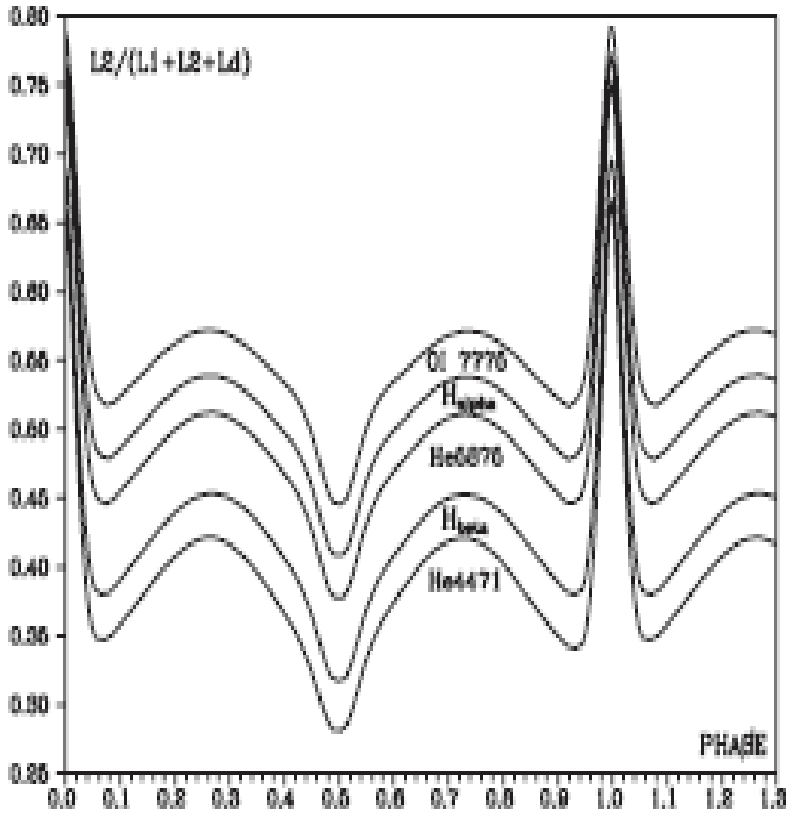

Figure 5. Light contribution factor for the donor at different spectral lines and orbital phases according to the M12 model. L_1, L_2 and L_d are the gainer, donor and disc fluxes, respectively.

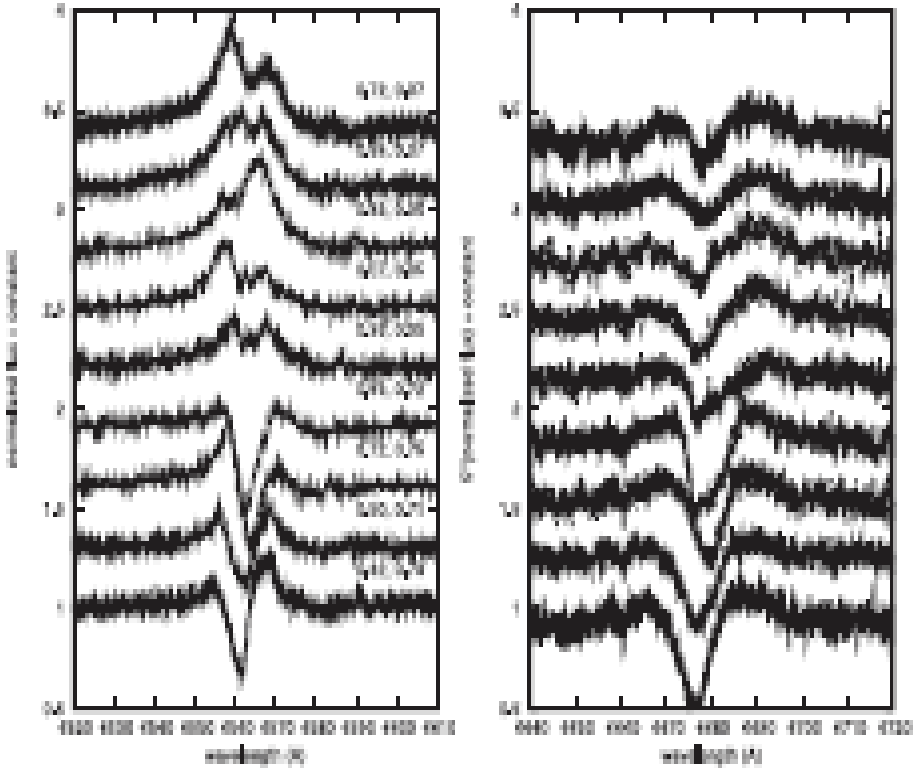

Figure 9. Donor-subtracted Hα (left) and He I 6678 (right) spectra at selected epochs. Orbital phases (left) and long-cycle phases (right) are given. Note the C I 6588 emission redward Hα.

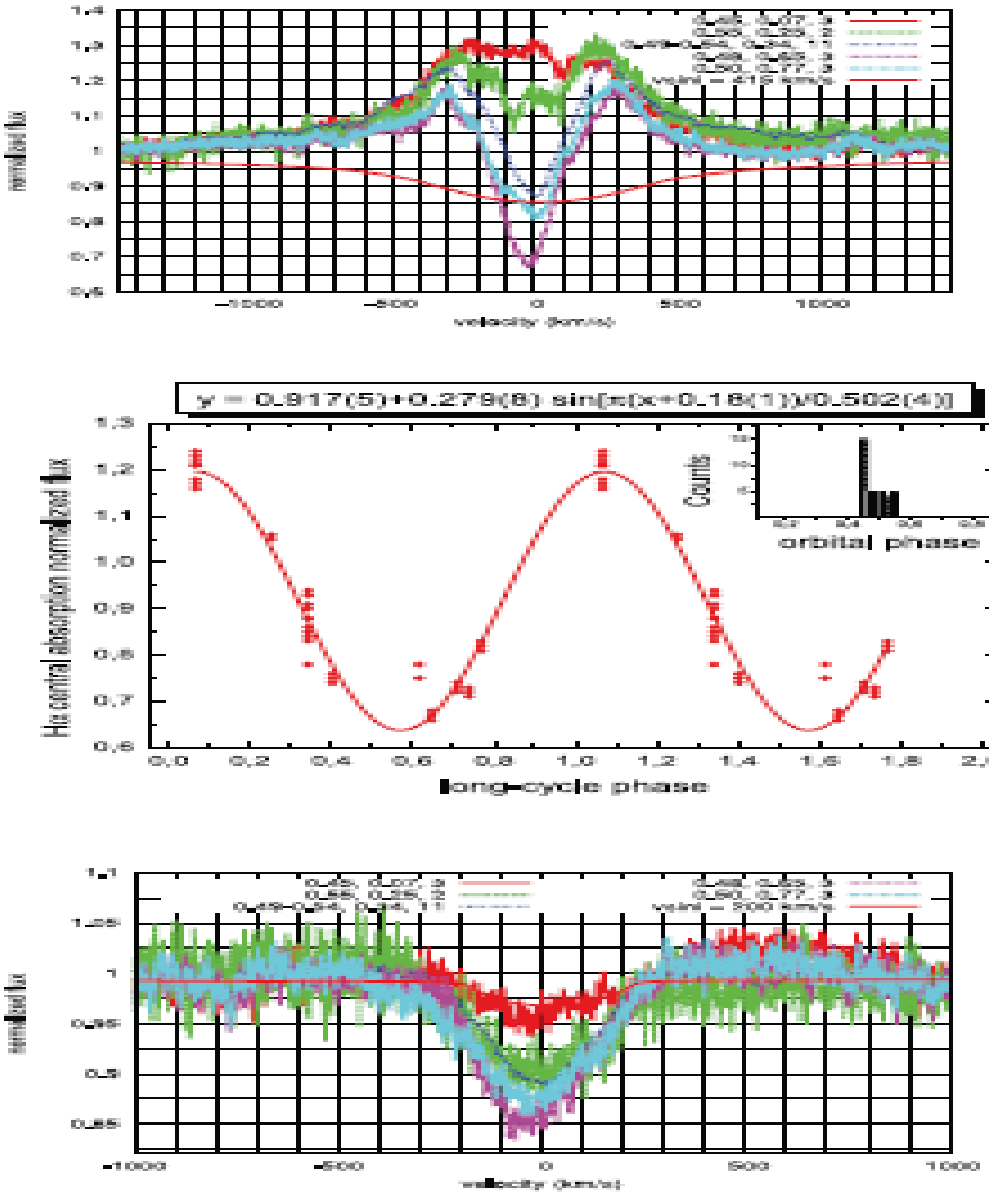

Figure 8. Up and down: donor-subtracted Hα and He I 6678 profiles near the secondary eclipse at different long-cycle phases. The labels indicate, from left to right, the orbital phase, long-cycle phase and number of spectra averaged. The synthetic profiles of the gainer calculated with parameters given by M12 are shown for different rotational velocities. *X*-axis velocities are with respect to the system centre of mass. Middle: the behaviour of the intensity of the CA of the donor-subtracted Hα profile at the secondary eclipse during the long cycle. The best sinus fit is also shown along with the histogram of orbital phases for the considered spectra.

MNRAS 428, 1594–1605 (2013) doi:10.1093/mnras/sts143

Physical parameters and evolutionary route for the Large Magellanic Cloud interacting binary OGLE 05155332−6925581★

H. E. Garrido,[1,2] R. E. Mennickent,[2†] G. Djurašević,[3,4] Z. Kołaczkowski,[5] E. Niemczura[5] and N. Mennekens[6]

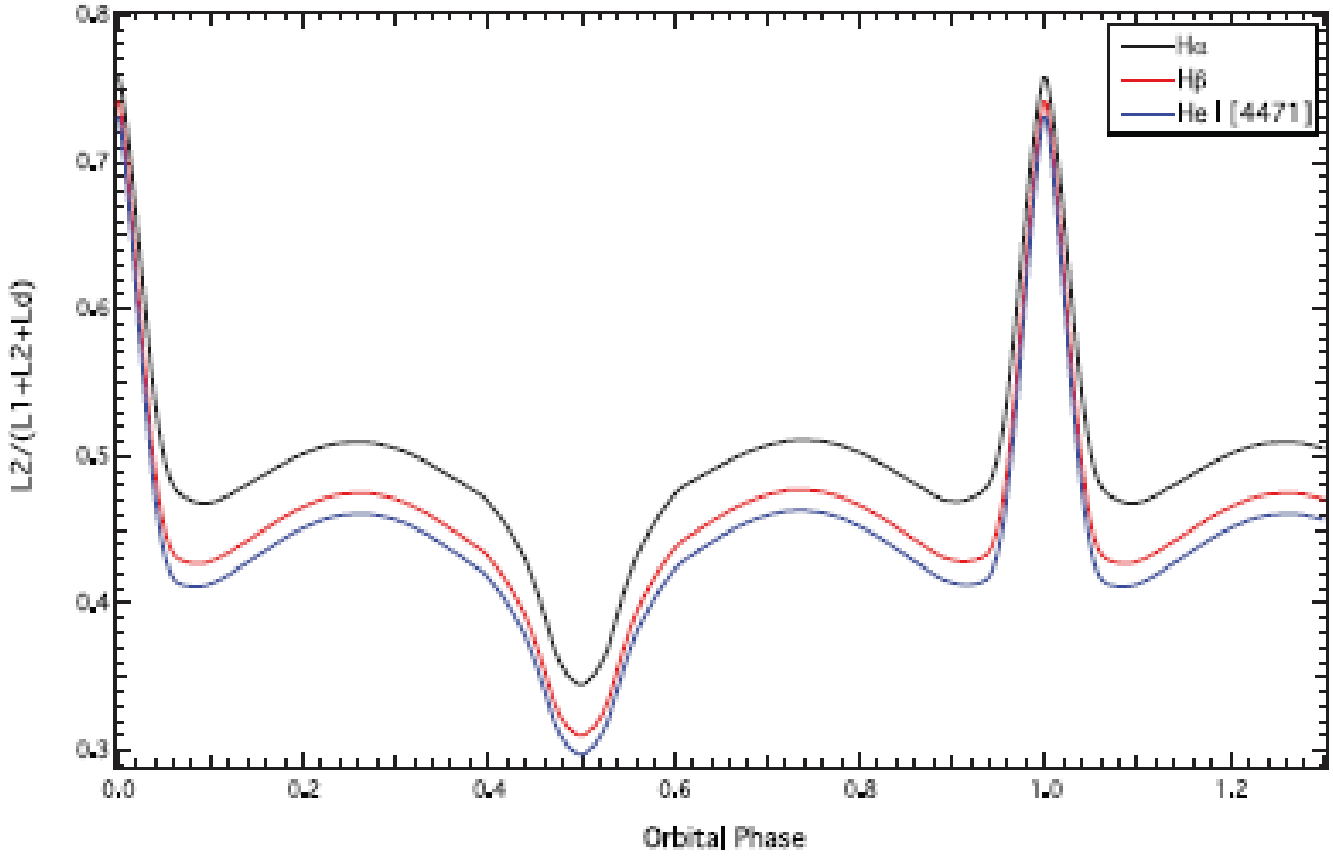

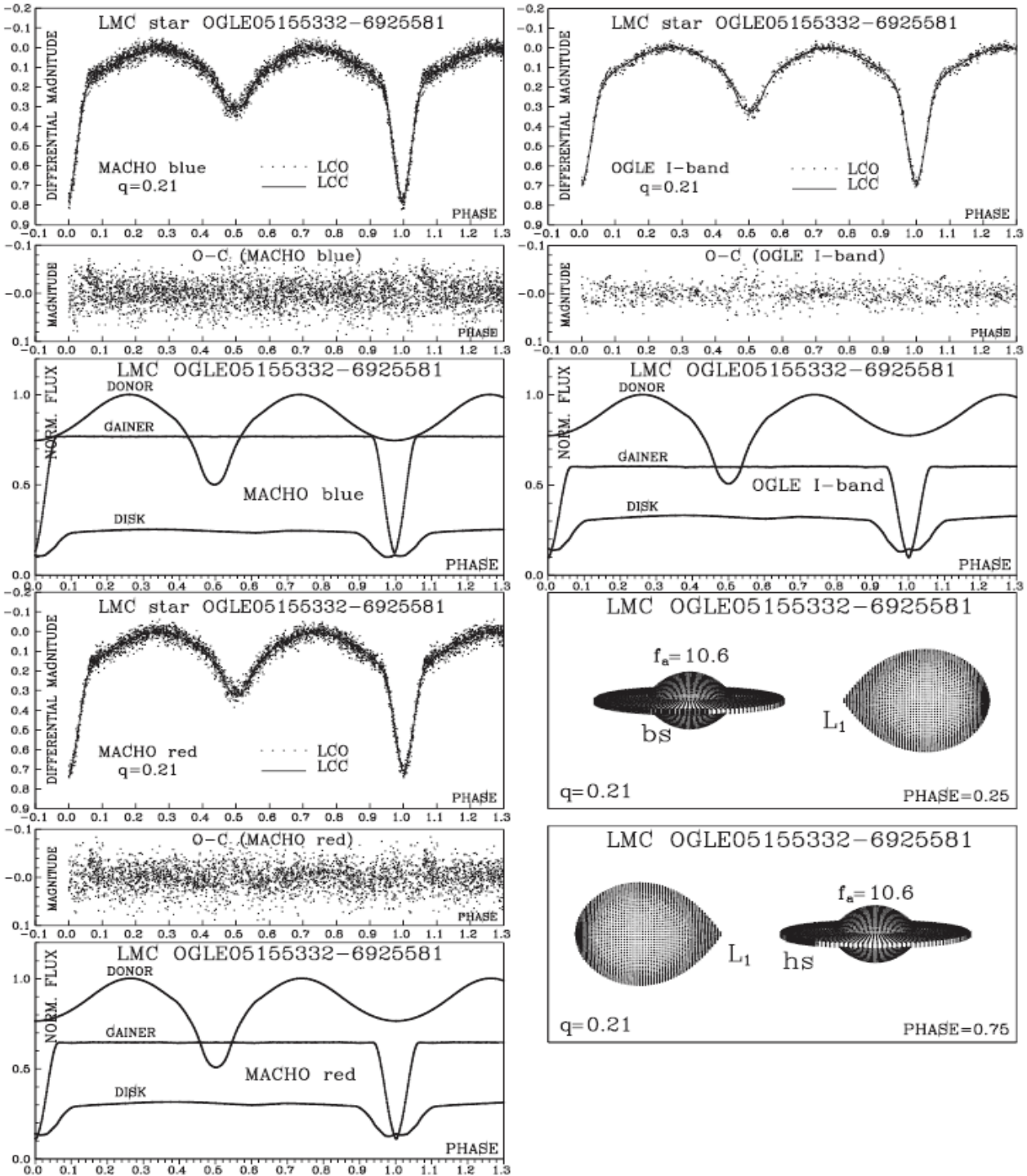
LMC star OGLE05155332-6925581
DIFFERENTIAL MAGNITUDE
MACHO blue
q=0.21
LCO
LCC
PHASE
LMC star OGLE05155332-6925581
DIFFERENTIAL MAGNITUDE
OGLE I-band
q=0.21
LCO
LCC
PHASE
O-C (MACHO blue)
MAGNITUDE
PHASE
O-C (OGLE I-band)
MAGNITUDE
PHASE
LMC OGLE05155332-6925581
NORM. FLUX
DONOR
GAINER
MACHO blue
DISK
PHASE
LMC OGLE05155332-6925581
NORM. FLUX
DONOR
GAINER
OGLE I-band
DISK
PHASE
LMC star OGLE05155332-6925581
DIFFERENTIAL MAGNITUDE
MACHO red
q=0.21
LCO
LCC
PHASE
LMC OGLE05155332-6925581
f_a=10.6
bs
L_1
q=0.21
PHASE=0.25
O-C (MACHO red)
MAGNITUDE
PHASE
LMC OGLE05155332-6925581
NORM. FLUX
DONOR
GAINER
MACHO red
DISK
PHASE
LMC OGLE05155332-6925581
L_1
f_a=10.6
hs
q=0.21
PHASE=0.75

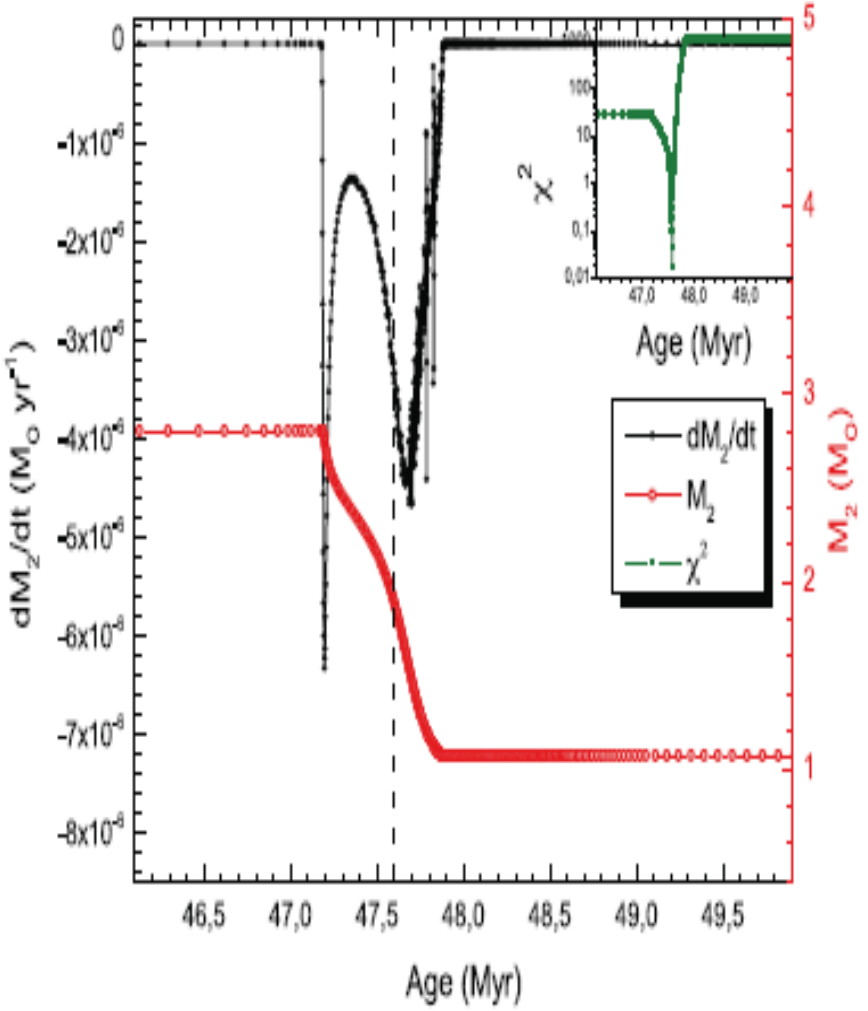

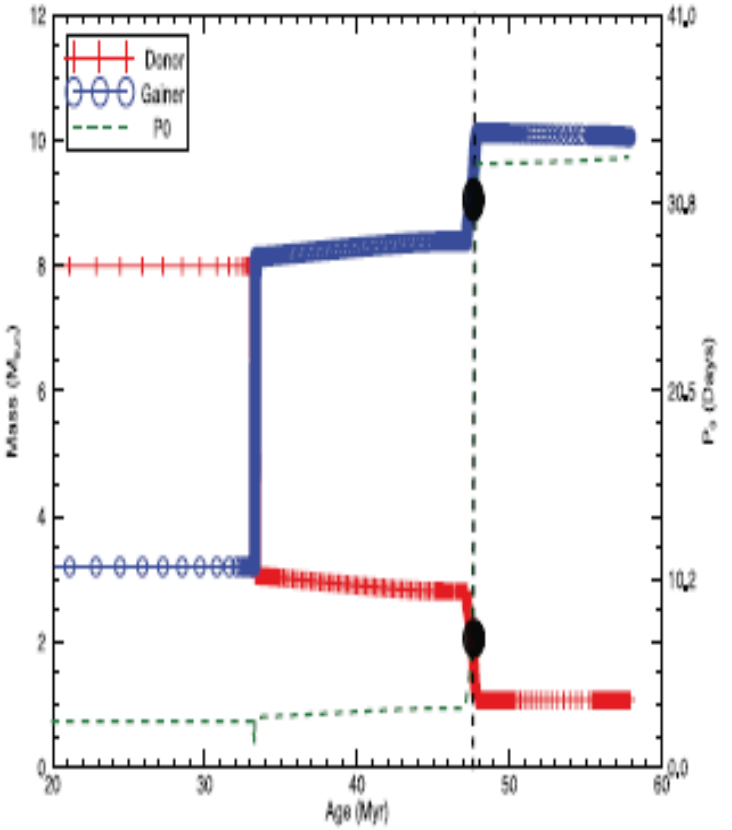

Figure 8. Left: $\dot{M}_2$ (upper curve) and M_2 for the best evolutionary model; χ^2 is shown in the inset graph. The few spikes in the $\dot{M}_2$ curve reflect minor convergence artefacts produced during the numerical calculations. Right: evolution of orbital period and mass of the components with the mass transfer time for OGLE 05155332−6925581 with the initial orbital period $P_{\mathrm{orb,i}} = 2.5$ d. The vertical dashed lines and filled circles indicate the position for the best model.

MNRAS 448, 1137–1152 (2015) doi:10.1093/mnra

Fundamental parameters of the close interacting binary HD 170582 and its luminous accretion disc

R. E. Mennickent,[1]★ G. Djurašević,[2] M. Cabezas,[1] A. Cséki,[2] J. G. Rosales,[1] E. Niemczura,[3] I. Araya[4] and M. Curé[4]

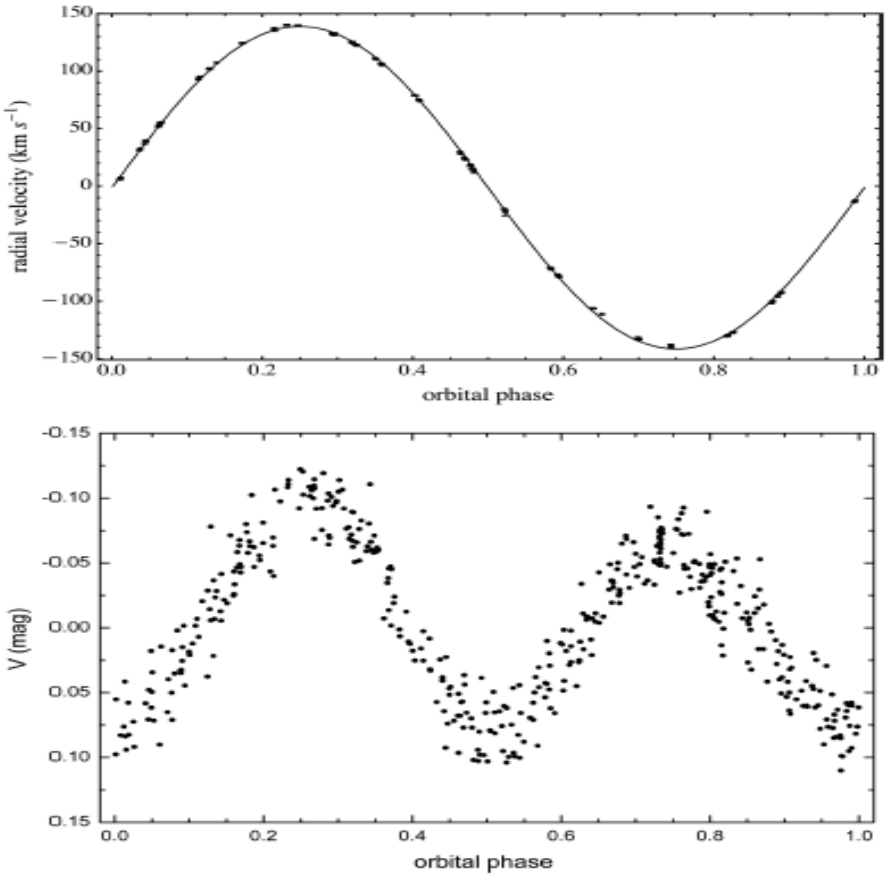

Figure 5. Upper panel: the donor RVs and the best fit, given by equation (4) and the parameters of Table 4. The RV error bars are also shown, but they are usually smaller than the used symbols. Lower panel: disentangled orbital light curve. In both panels phases are calculated according to times of donor inferior conjunction, given by equation (7).

$$\frac{v_{2r}\sin i}{K_2} \approx (1+q)\frac{0.49q^{2/3}}{0.6q^{2/3}+\ln(1+q^{1/3})}$$

The system mass function for a binary in a circular orbit can be expressed as

$$f = \frac{M_2 \sin^3 i}{q(1+q)^2} = 1.0361 \times 10^{-7}\left(\frac{K_2}{\mathrm{km\ s^{-1}}}\right)^3 \frac{P_o}{\mathrm{day}}\mathrm{M}_\odot. \qquad (10)$$

The f value derived from our RV study is 4.81 ± 0.01 M$_\odot$. Using $q = 0.21$ (donor rotating synchronously), we get $M_2 > 1.48$ M$_\odot$ and $M_1 > 7.05$ M$_\odot$. On the other hand, if $q = 0.54$ we derive $M_2 > 6.16$ M$_\odot$ and $M_1 > 11.41$ M$_\odot$. These masses turns to be too high for the temperatures derived from spectroscopy and this fact supports the $q = 0.21$ solution.

Table 9. Results of the analysis of HD170582 V-band light curve obtained by solving the inverse problem for the Roche model with an accretion disc around the more-massive (hotter) gainer in synchronous rotation regime. Symbols are as in Table 6 but the gainer temperature is 21 000 K.

Quantity		Quantity	
n	455	$\mathcal{M}_1\,[\mathrm{M}_\odot]$	9.0 ± 0.2
$\Sigma(O-C)^2$	0.1516	$\mathcal{M}_2\,[\mathrm{M}_\odot]$	1.9 ± 0.1
σ_{rms}	0.0183	$\mathcal{R}_1\,[\mathrm{R}_\odot]$	5.5 ± 0.2
$i[^\circ]$	67.4 ± 0.4	$\mathcal{R}_2\,[\mathrm{R}_\odot]$	15.6 ± 0.2
F_{d}	0.66 ± 0.02	$\log g_1$	3.9 ± 0.1
T_{d}[K]	5430 ± 200	$\log g_2$	2.33 ± 0.1
$d_{\mathrm{e}}[a_{\mathrm{orb}}]$	0.156 ± 0.004	M^1_{bol}	-4.5 ± 0.2
$d_{\mathrm{c}}[a_{\mathrm{orb}}]$	0.038 ± 0.004	M^2_{bol}	-2.6 ± 0.1
a_{T}	8.5 ± 0.4	$a_{\mathrm{orb}}\,[\mathrm{R}_\odot]$	61.2 ± 0.2
f_1	1.00	$\mathcal{R}_{\mathrm{d}}\,[\mathrm{R}_\odot]$	21.2 ± 0.3
F_1	0.187 ± 0.004	$d_{\mathrm{e}}\,[\mathrm{R}_\odot]$	2.4 ± 0.1
T_1[K]	21000	$d_{\mathrm{c}}\,[\mathrm{R}_\odot]$	9.6 ± 0.1
T_2[K]	8000		
$A_{\mathrm{hs}} = T_{\mathrm{hs}}/T_{\mathrm{d}}$	1.85 ± 0.1		
$\theta_{\mathrm{hs}}[^\circ]$	19.8 ± 2.0		
$\lambda_{\mathrm{hs}}[^\circ]$	330.6 ± 6.0		
$\theta_{\mathrm{rad}}[^\circ]$	10.0 ± 8.0		
$A_{\mathrm{bs}} = T_{\mathrm{bs}}/T_{\mathrm{d}}$	1.56 ± 0.1		
$\theta_{\mathrm{bs}}[^\circ]$	56.8 ± 3.0		
$\lambda_{\mathrm{bs}}[^\circ]$	103.7 ± 6.0		
Ω_1	11.25 ± 0.04		
Ω_2	2.26 ± 0.02		

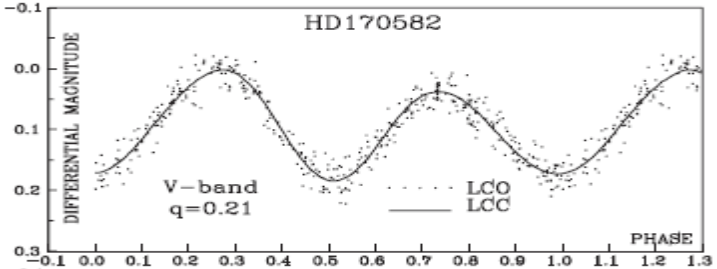

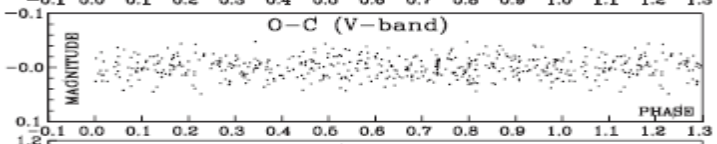

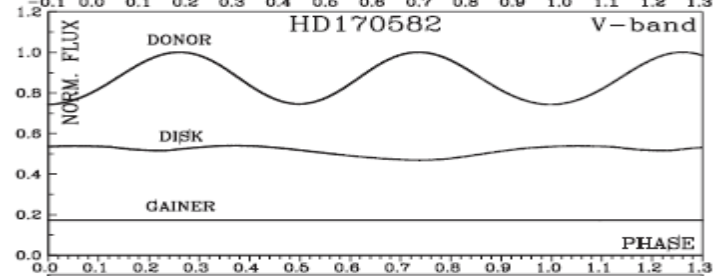

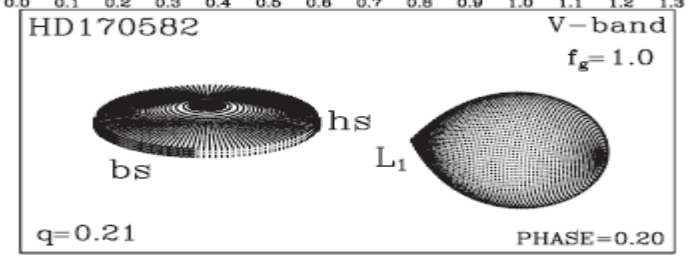

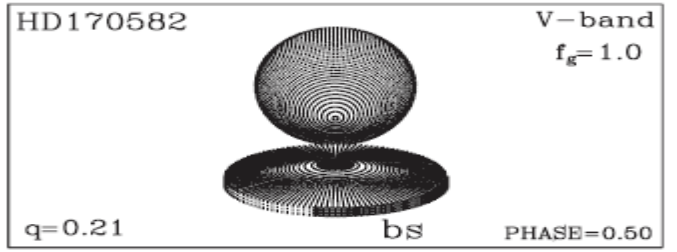

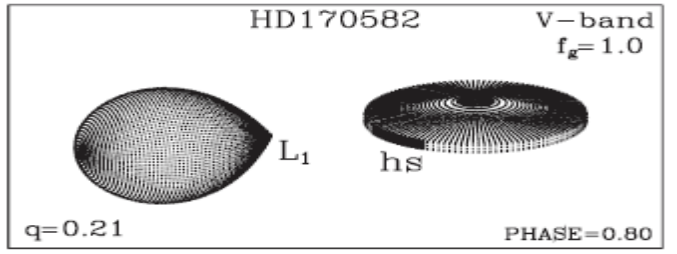

MNRAS 476, 3039–3050 (2018)
Advance Access publication 2018 January 29
doi:10.1093/mnras/sty224

Spectroscopic and photometric study of the eclipsing interacting binary V495 Centauri

J. A. Rosales Guzmán,[1★] R. E. Mennickent,[1★] G. Djurašević,[2,3] I. Araya[4,5] and M. Curé[4]

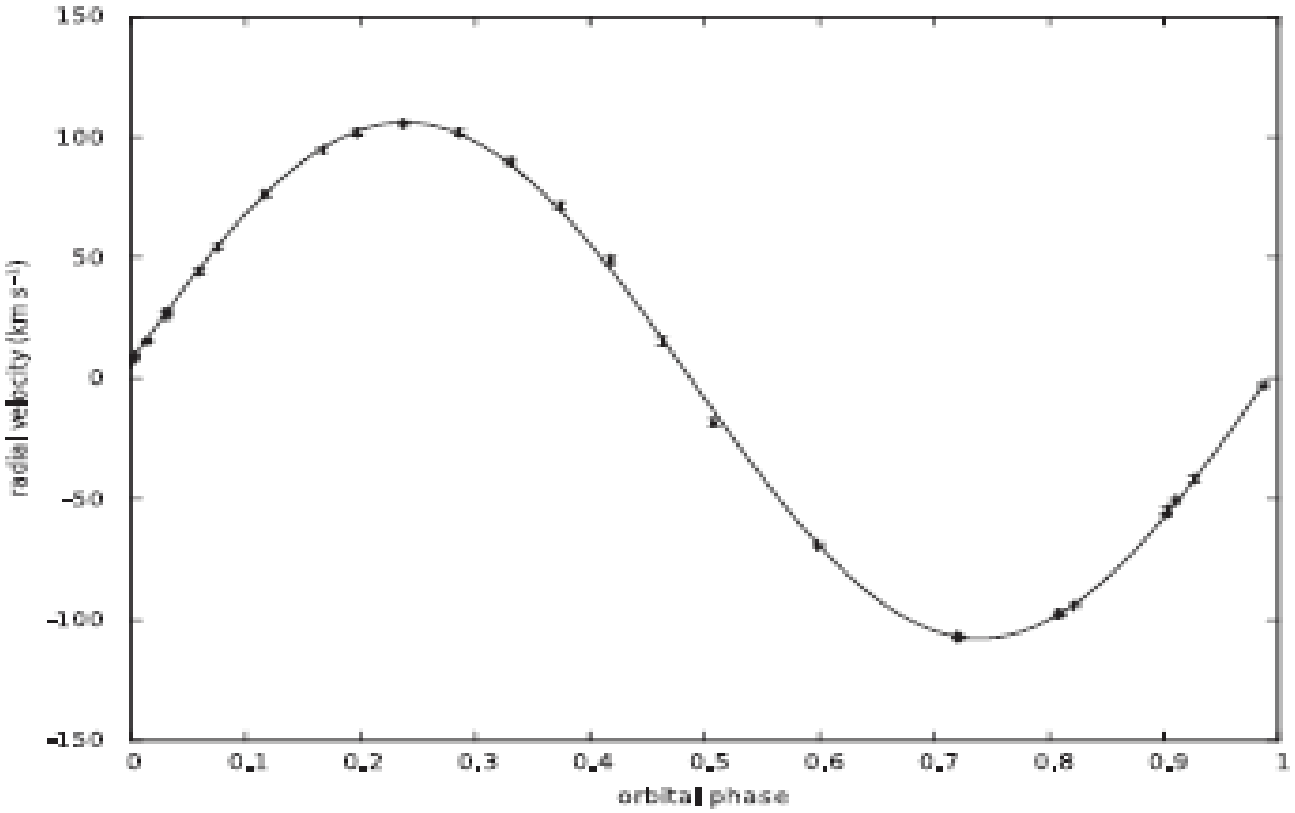

Figure 6. The radial velocities of the donor obtained by cross-correlation of a region plenty of metallic lines and the best fit, given for equation (4).

Table 6. Results of the analysis of the *V*-band light curve of V495 Cen obtained by solving the inverse problem for the Roche model with an accretion disc around the more-massive (hotter) gainer in the synchronous rotation regime.

Quantity		Quantity	
n	617	$\mathcal{M}_h[\mathcal{M}_\odot]$	5.76 ± 0.3
$\Sigma(O-C)^2$	0.5751	$\mathcal{M}_c[\mathcal{M}_\odot]$	0.91 ± 0.2
σ_{rms}	0.0306	$\mathcal{R}_h[R_\odot]$	4.5 ± 0.2
$i[^\circ]$	84.8 ± 0.6	$\mathcal{R}_c[R_\odot]$	19.3 ± 0.5
F_d	0.88 ± 0.03	$\log g_h$	3.89 ± 0.02
T_d[K]	4040 ± 250	$\log g_c$	1.83 ± 0.02
$d_e[a_{orb}]$	0.046 ± 0.016	M^h_{bol}	-3.16 ± 0.1
$d_c[a_{orb}]$	0.007 ± 0.009	M^c_{bol}	-1.80 ± 0.1
a_T	4.1 ± 0.3	$a_{orb}[R_\odot]$	82.8 ± 0.3
f_h	1.00	$\mathcal{R}_d[R_\odot]$	40.2 ± 1.3
F_h	0.109 ± 0.014	$d_e[R_\odot]$	3.8 ± 0.2
T_h[K]	16960 ± 400	$d_c[R_\odot]$	0.6 ± 0.2
$A_{hs} = T_{hs}/T_d$	1.11 ± 0.05		
$\theta_{hs}[^\circ]$	18.2 ± 2.0		
$\lambda_{hs}[^\circ]$	338.3 ± 9.0		
$\theta_{rad}[^\circ]$	-15.4 ± 13.6		
Ω_h	18.36 ± 0.02		
Ω_c	2.125 ± 0.05		

Note: *Fixed Parameters*: $q = \mathcal{M}_c/\mathcal{M}_h = 0.158$ – mass ratio of the components, $T_c = 6000$ K – temperature of the less-massive (cooler) donor, $F_c = 1.0$ – filling factor for the critical Roche lobe of the donor, $f_{h,c} = 1.00$ – non-synchronous rotation coefficients of the system components, $\beta_h = 0.25$, $\beta_c = 0.08$ – gravity-darkening coefficients of the components, $A_h = 1.0$, $A_c = 0.5$ – albedo coefficients of the components.

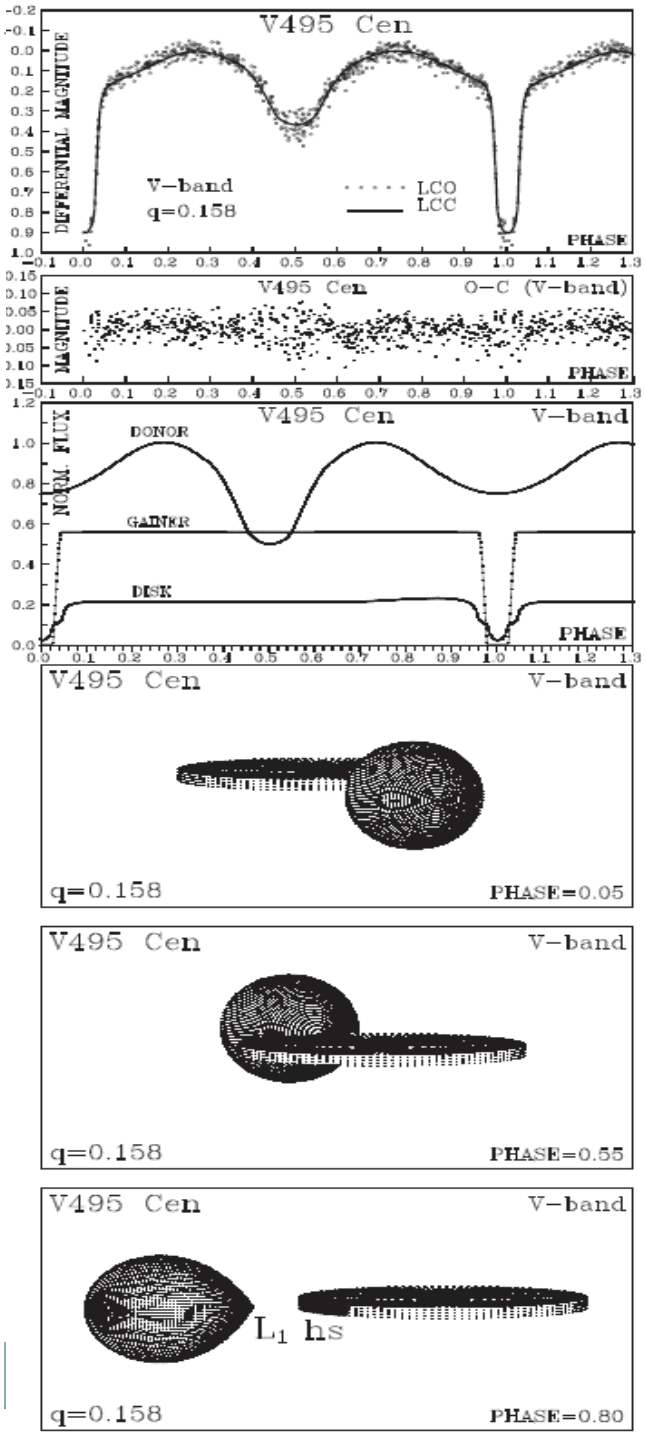

A&A 552, A63 (2013)
DOI: 10.1051/0004-6361/201220230

Astronomy & Astrophysics

Fundamental stellar and accretion disc parameters of the eclipsing binary DQ Velorum*

D. Barrfa[1,2], R. E. Mennickent[1], L. Schmidtobreick[2], G. Djurašević[3,4], Z. Kołaczkowski[5], G. Michalska[5], M. Vučković[2,3], and E. Niemczura[6]

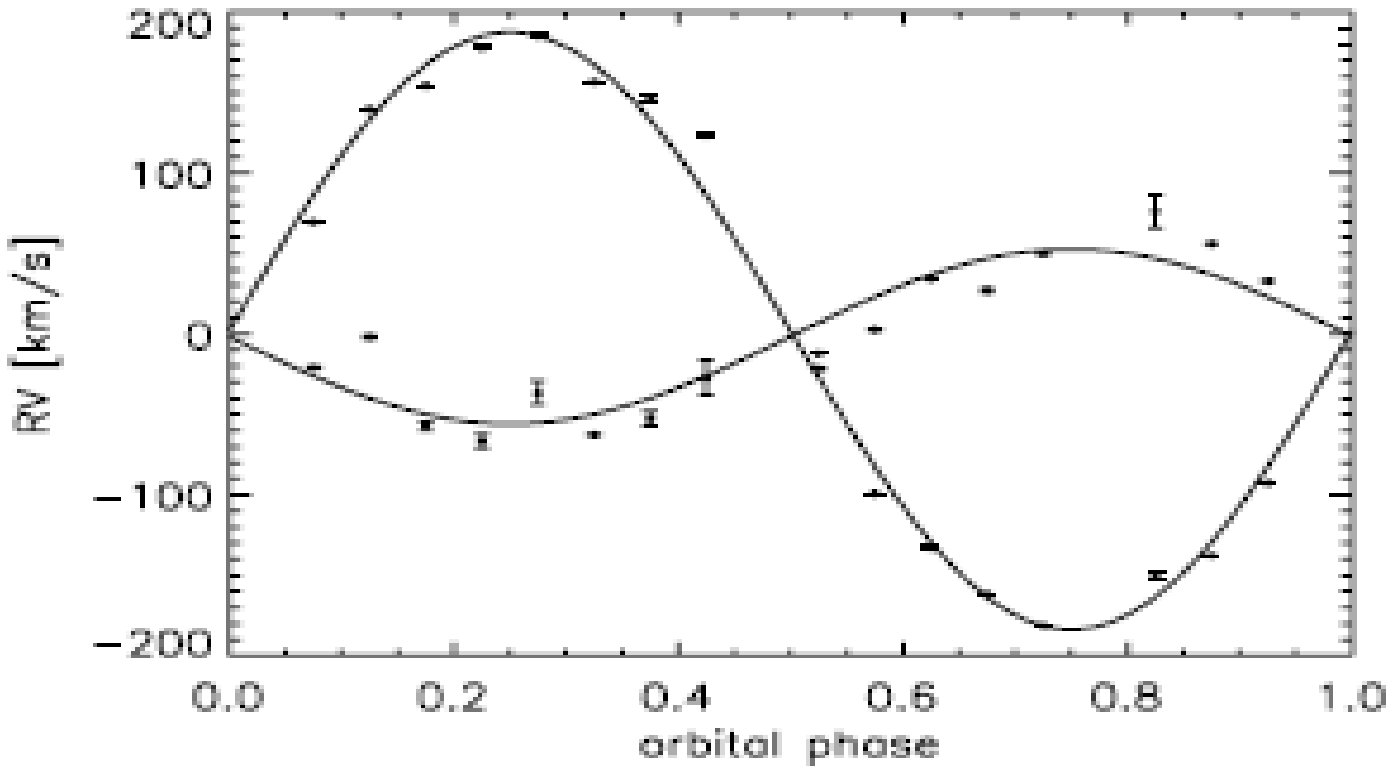

Fig. 3. RV curves and best sinus fit for DQ Vel components. Each RV was measured from Table 3 and Table 4 taking the mean value in orbital phase bins of 0.05.

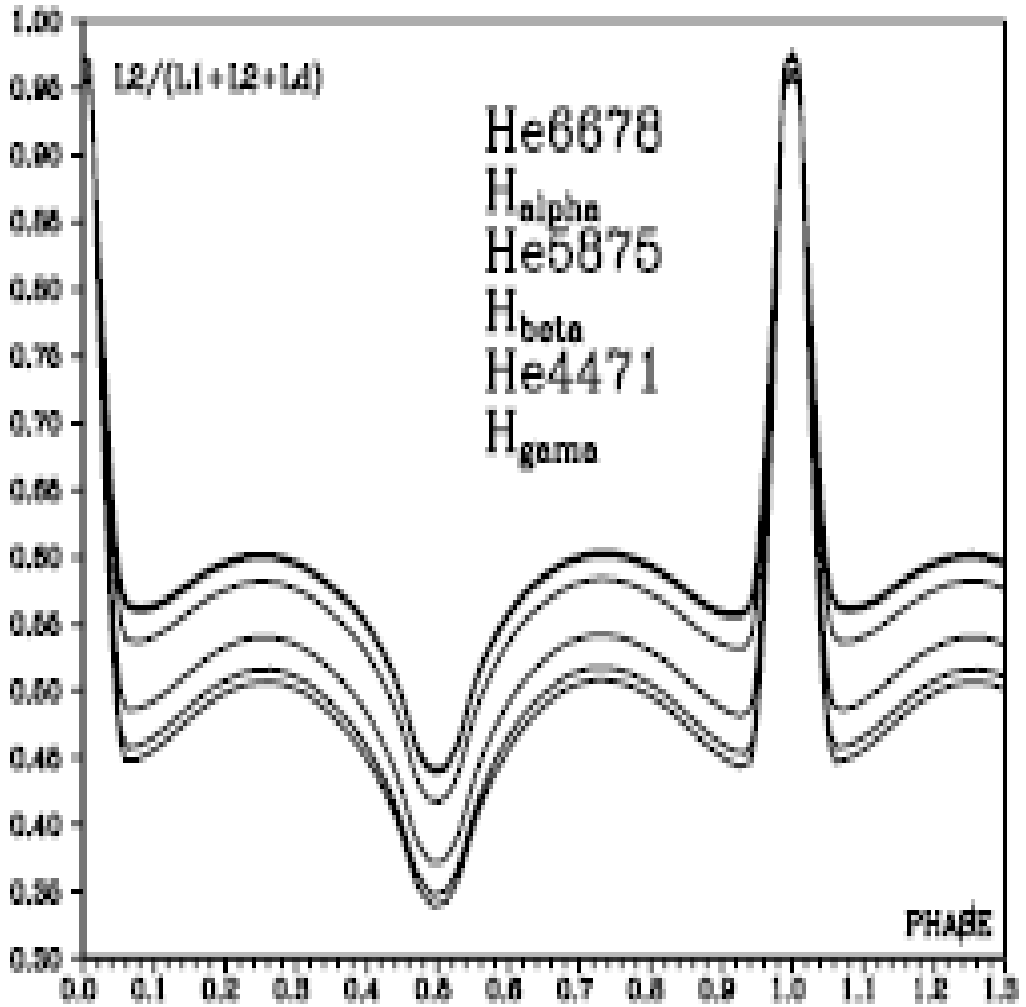

Fig. 5. Donor light contribution with respect to the total light calculated from the light curve model. Each curve shows the donor contribution for a specific spectral range around a spectral line. The selected spectral lines (and ranges) are from top to the bottom: HeI 6678 Å, Hα, HeI 5875 Å, Hβ, HeI 4471 Å, and Hγ. L1 and L2 are the stellar fluxes and Ld is the disc contribution.

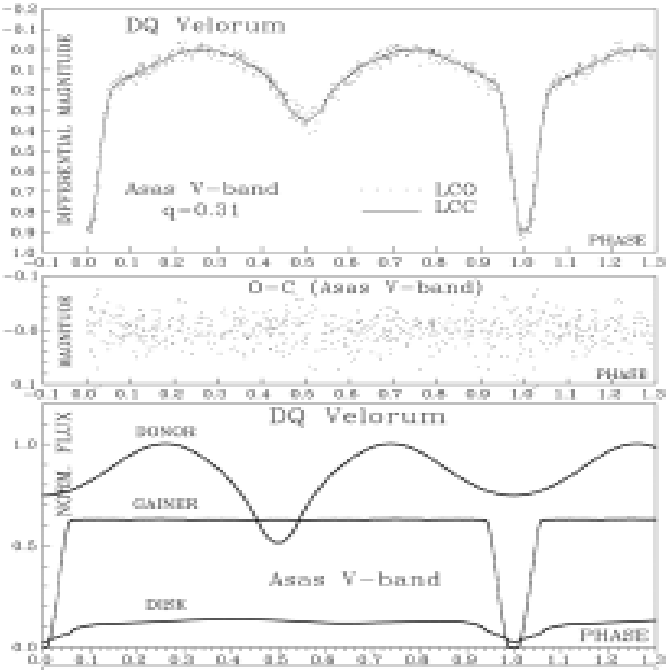

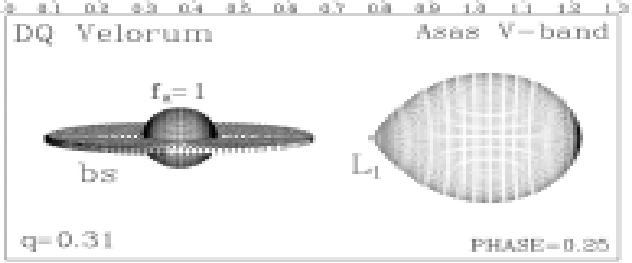

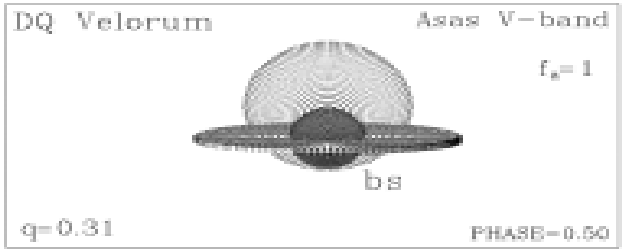

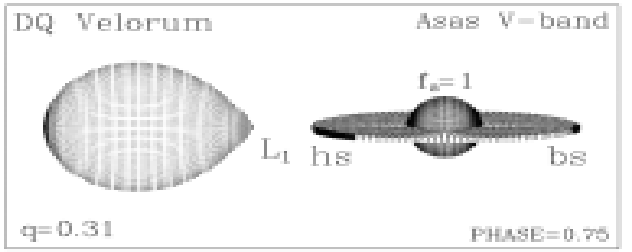

MNRAS 432, 799–809 (2013)
Advance Access publication 2013 April 19

On the accretion disc and evolutionary stage of β Lyrae

R. E. Mennickent[1]★ and G. Djurašević[2,3]

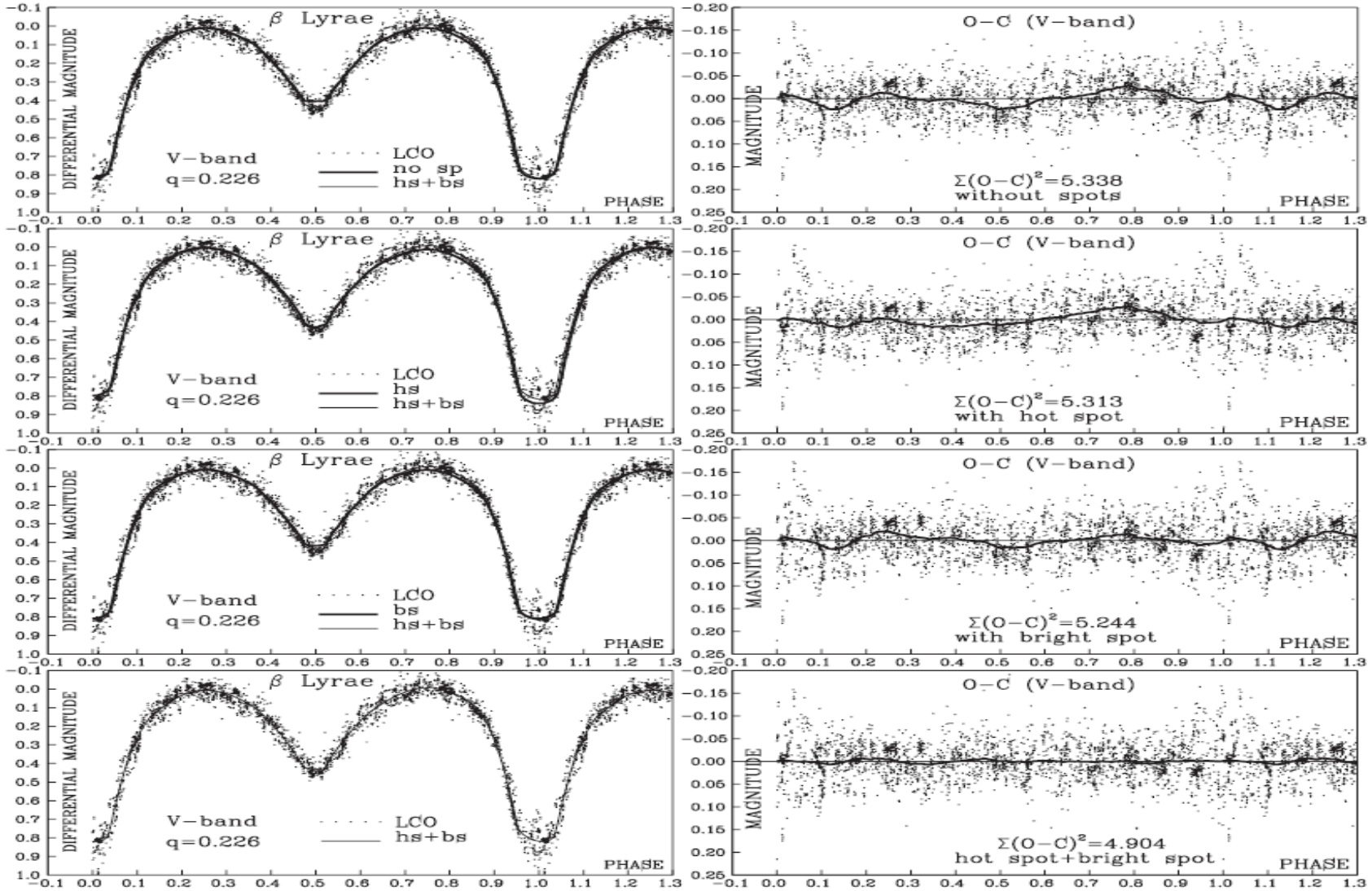

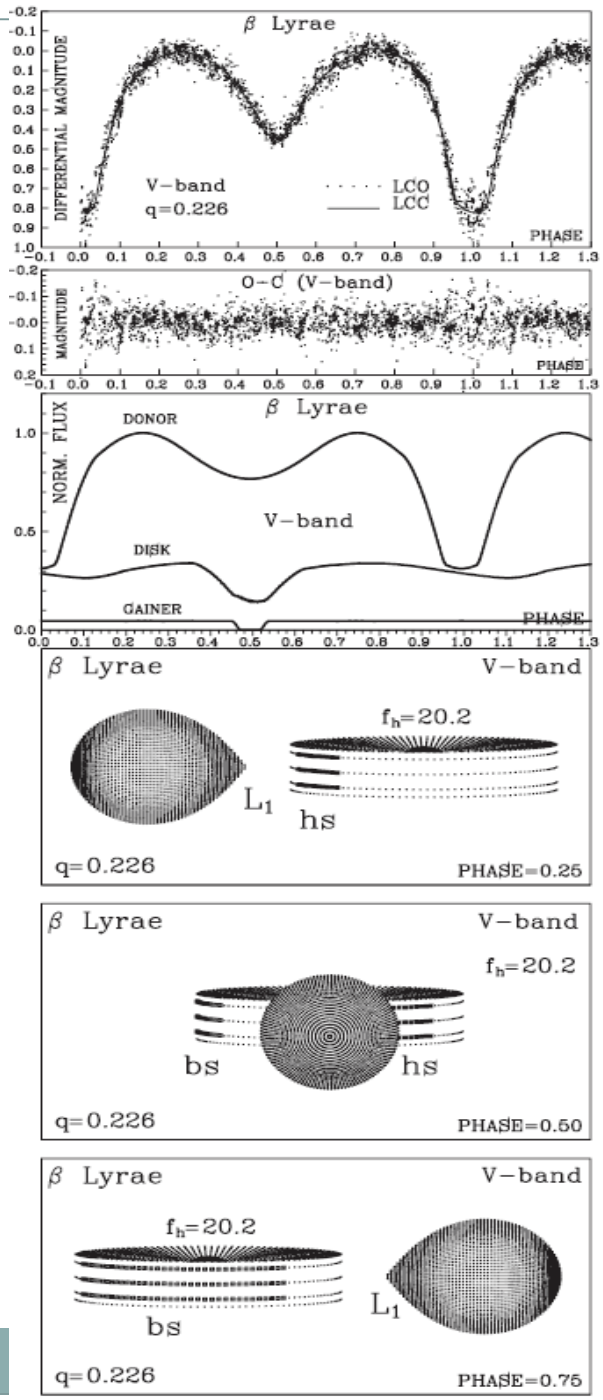

Table 1. Parameters of the best-fitting model for the β Lyr V-band LC obtained by solving the inverse problem considering an accretion disc around a gainer in critical rotation regime.

Quantity		Quantity	
n	2852	$\mathcal{M}_h(\mathcal{M}_\odot)$	13.16 ± 0.3
$\Sigma(O-C)^2$	4.9040	$\mathcal{M}_c(\mathcal{M}_\odot)$	2.97 ± 0.2
σ_{rms}	0.0415	$\mathcal{R}_h(R_\odot)$	6.0 ± 0.2
$i(^\circ)$	86.1 ± 0.5	$\mathcal{R}_c(R_\odot)$	15.2 ± 0.2
F_d	0.94 ± 0.03	$\log_{10} g_h$	4.0 ± 0.1
T_d(K)	8200 ± 400	$\log_{10} g_c$	2.5 ± 0.1
$d_e(a_{orb})$	0.192 ± 0.009	M^h_{bol}	-6.3 ± 0.2
$d_c(a_{orb})$	0.01 ± 0.01	M^c_{bol}	-4.7 ± 0.1
a_T	3.8 ± 0.3	$a_{orb}(R_\odot)$	58.5 ± 0.3
f_h	20.2 ± 0.5	$\mathcal{R}_d(R_\odot)$	28.3 ± 0.3
F_h	1.00	$d_e(R_\odot)$	11.2 ± 0.2
T_h(K)	$30\,000 \pm 2000$	$d_c(R_\odot)$	0.6 ± 0.1
$A_{hs} = T_{hs}/T_d$	1.21 ± 0.1	$\log_{10} T_h$	4.48
$\theta_{hs}(^\circ)$	16.2 ± 2.0	$\log_{10} T_c$	4.12
$\lambda_{hs}(^\circ)$	324.6 ± 7.0	$\log_{10} L_h$	4.42
$\theta_{rad}(^\circ)$	-13.5 ± 5.0	$\log_{10} L_c$	3.81
$A_{bs} = T_{bs}/T_d$	1.12 ± 0.1		
$\theta_{bs}(^\circ)$	53.8 ± 5.0		
$\lambda_{bs}m(^\circ)$	107.3 ± 9.0		
$A_{h,\,c,\,d}$	0.10, 0.35, 0.59		
Ω_h	12.12 ± 0.02		
Ω_c	2.296 ± 0.02		

Fixed parameters: $q = \mathcal{M}_c/\mathcal{M}_h = 0.226$ – mass ratio of the components, $T_c = 13300$ K – temperature of the less-massive (cooler) donor, $F_c = 1.0$ – filling factor for the critical Roche lobe of the donor, $F_h = R_h/R_{zc} = 1.0$ – filling factor for the critical non-synchronous lobe of the hotter, more massive gainer (ratio of the stellar polar radius to the critical non-synchronous lobe radius along z-axis for a star in critical rotation regime), $f_c = 1.00$ – non-synchronous rotation coefficients of the donor, $\beta_{h,c} = 0.25$ – gravity-darkening coefficients of the components.

Note: n – number of observations, $\Sigma(O-C)^2$ – final sum of squares of residuals between observed (LCO) and synthetic (LCC) LCs, σ_{rms} – root-mean-square of the residuals, i – orbit inclination (in arc degrees), $F_d = R_d/R_{yc}$ – disc dimension factor (the ratio of the disc radius to the critical Roche lobe radius along y-axis), T_d – disc-edge temperature, d_e, d_c, – disc thicknesses (at the edge and at the centre of the disc, respectively) in the units of the distance between the components, a_T – disc temperature distribution coefficient, f_h – non-synchronous rotation coefficient of the more massive gainer (in the critical rotation regime), T_h – temperature of the gainer, $A_{hs,bs} = T_{hs,bs}/T_d$ – hot and bright spots' temperature coefficients, $\theta_{hs,bs}$ and $\lambda_{hs,bs}$ – spots' angular dimensions (radius) and longitudes (in arc degrees), θ_{rad} – angle between the line perpendicular to the local disc edge surface and the direction of the hotspot maximum radiation, $A_{h,\,c,\,d}$ – albedo coefficients of the system components and the accretion disc, $\Omega_{h,c}$ – dimensionless surface potentials of the hotter gainer and cooler donor, $\mathcal{M}_{h,c}(\mathcal{M}_\odot)$, $\mathcal{R}_{h,c}(R_\odot)$ – stellar masses and mean radii of stars in solar units, $\log_{10} g_{h,c}$ – logarithm (base 10) of the system components effective gravity, $M^{h,c}_{bol}$ – absolute stellar bolometric magnitudes, a_{orb} $(R_\odot)$, $\mathcal{R}_d(R_\odot)$, $d_e(R_\odot)$, $d_c(R_\odot)$ – orbital semimajor axis, disc radius and disc thicknesses at its edge and centre, respectively, given in solar units, $\log_{10} T_{h,c}$, $\log_{10} L_{h,c}$ – logarithm (base 10) of the system components effective temperature and luminosity.

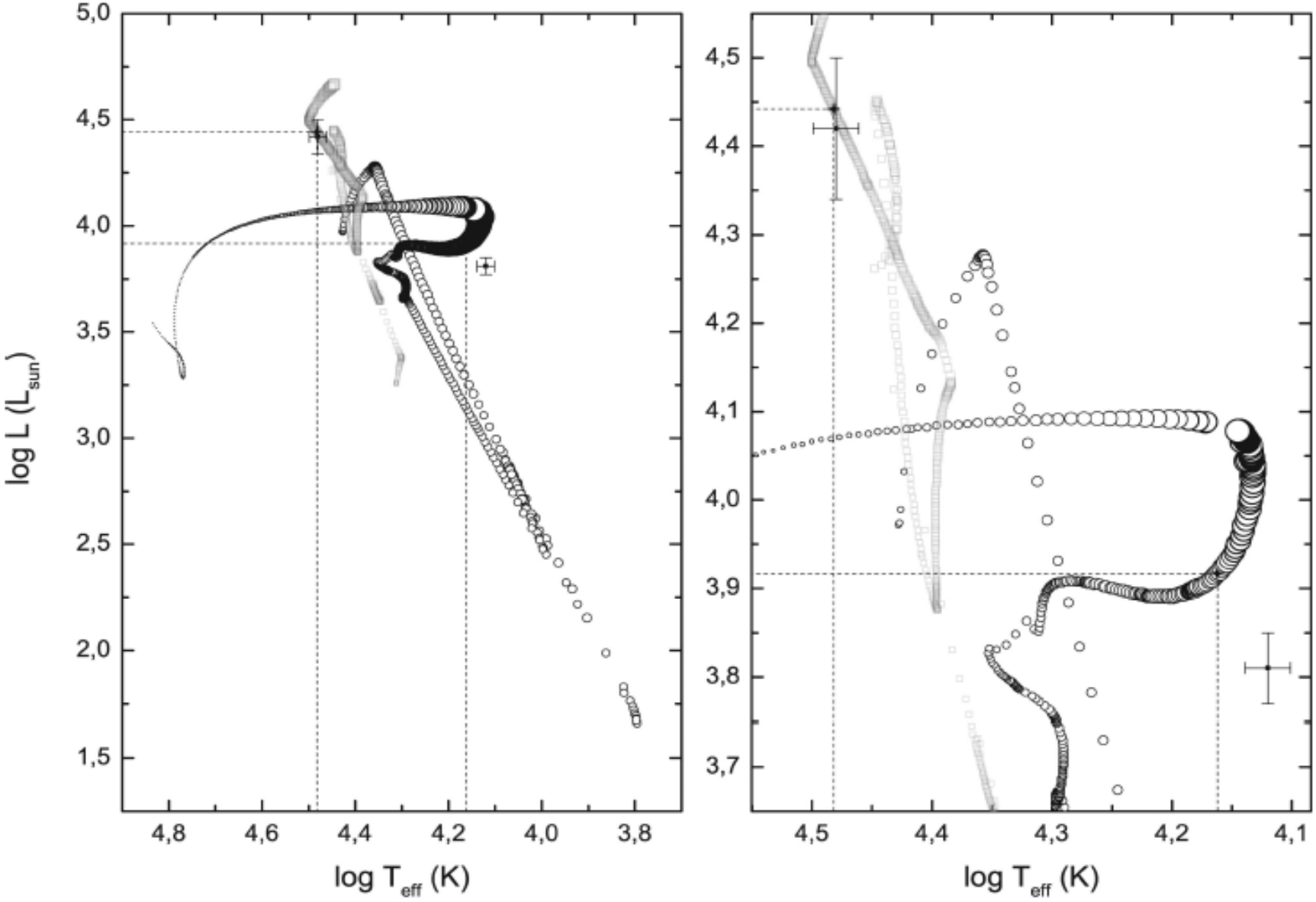

Figure 5. Evolutionary tracks for the binary star model from Van Rensbergen et al. (2008) that best fit the data. Donor (right black track) and gainer (left grey track) evolutionary paths are shown, along with the parameters derived from the LC fit. The best fit is reached at the time corresponding to the model attached to the axis by dashed lines, that is characterized in Table 2. The mismatch for the donor is discussed in the text. Stellar sizes are proportional to the circle diameters. An expanded view is shown in the right-hand panel where half of the points are shown for the donor track for best visualization.

MNRAS 477, L11–L15 (2018)
Advance Access publication 2018 March 14
doi:10.1093/mnrasl/sly042

Structural changes in the hot Algol OGLE-LMC-DPV-097 and its disc related to its long cycle

J. Garcés L.,[1★] R. E. Mennickent,[1★] G. Djurašević,[2,3] R. Poleski,[4,5] and I. Soszyński[4]

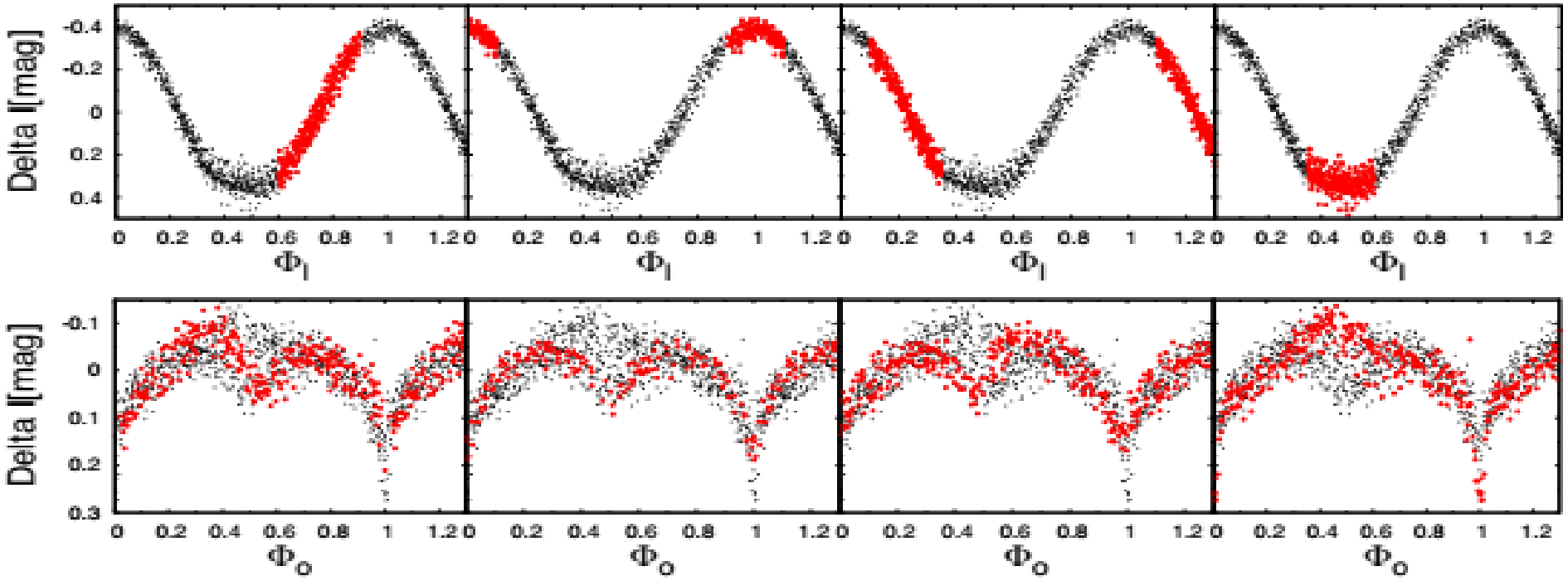

Figure 1. Disentangled long-cycle (up) and orbital (down) light curves phased with the respective periods. Black dots show the complete data set, red dots show segments of the data of the long cycle. It is evident the change in orbital light-curve shape at different long-cycle phases.

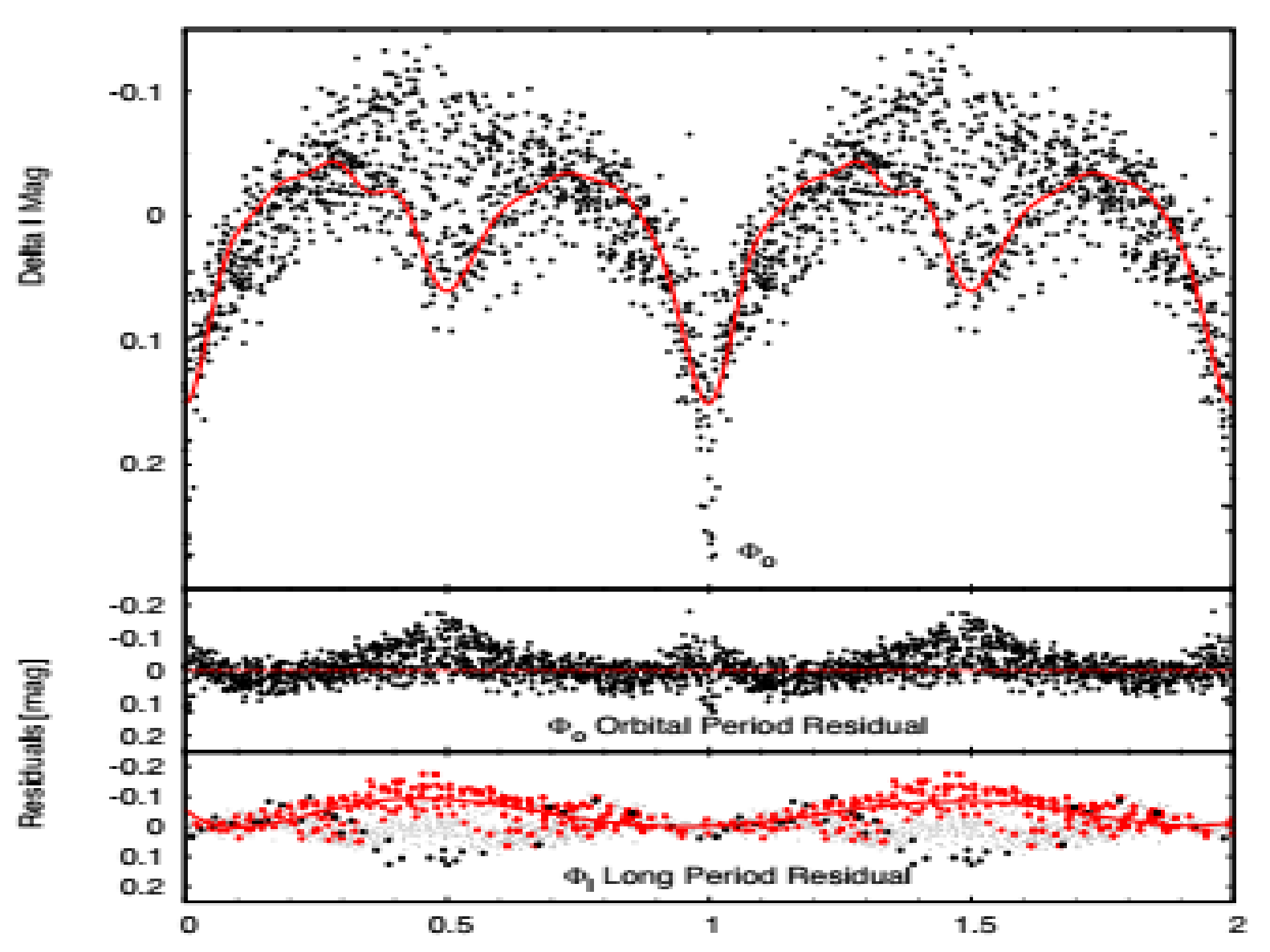
Delta I [Mag]
-0.1
0
0.1
0.2
Φ_0
Residuals [mag]
-0.2
-0.1
0
0.1
0.2
Φ_0 Orbital Period Residual
-0.2
-0.1
0
0.1
0.2
Φ_1 Long Period Residual
0
0.5
1
1.5
2

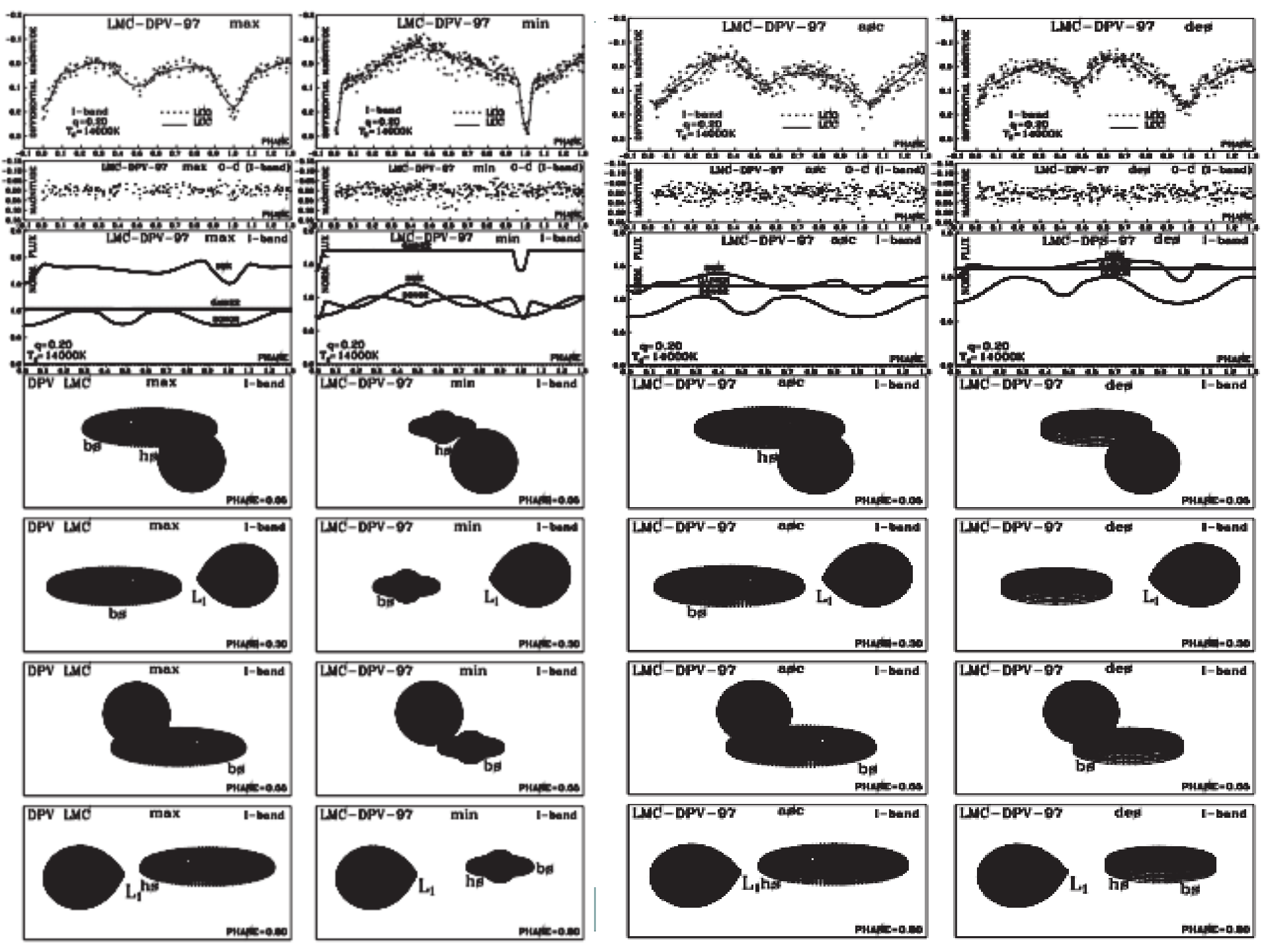
LMC-DPV-97 max
LMC-DPV-97 min
LMC-DPV-97 apic
LMC-DPV-97 dep
I-band
q=0.20
T2=14000K
LMC-DPV-97 max O-C (I-band)
LMC-DPV-97 min O-C (I-band)
LMC-DPV-97 apic O-C (I-band)
LMC-DPV-97 dep O-C (I-band)
LMC-DPV-97 max I-band
LMC-DPV-97 min I-band
LMC-DPV-97 apic I-band
LMC-DPV-97 dep I-band
DPV LMC max I-band
LMC-DPV-97 min I-band
LMC-DPV-97 apic I-band
LMC-DPV-97 dep I-band
bg
hg
L1
PHASE=0.00
PHASE=0.30
PHASE=0.50